New bis-pyrazolylpyridine ruthenium(III) complex as a potential anticancer drug: *In vitro* and *in vivo* activity in murine colon cancer

Dejan Lazić,[a] Andreas Scheurer,[b] Dušan Ćoćić,[c] Jelena Milovanović,[d,e] Aleksandar Arsenijević,[d] Bojana Stojanović,[d,f] Nebojša Arsenijević,[d] Marija Milovanović,*[d] and Ana Rilak Simović*[g]

[a]*Department of Surgery, Faculty of Medical Sciences, University of Kraujevac, Svetozara Markovića 69, 34000 Kragujevac, Serbia*

[b]*Inorganic Chemistry, Department of Chemistry and Pharmacy, University of Erlangen-Nürnberg, Erlangen, Germany.*

[c]*University of Kragujevac, Faculty of Science, Radoja Domanovića 12, P. O. Box 60, 34000 Kragujevac, Serbia.*

[d]*Center for Molecular Medicine and Stem Cell Research, Faculty of Medical Sciences, University of Kragujevac, Kragujevac, Serbia.*

[e]*Department of Histology, Faculty of Medical Sciences, University of Kragujevac, Serbia.*

[f]*Department of Pathophysiology, Faculty of Medical Sciences, University of Kragujevac, Serbia.*

[g]*University of Kragujevac, Institute for Information Technologies Kragujevac, Department of Natural Sciences, Jovana Cvijića bb, 34000 Kragujevac, Serbia.*

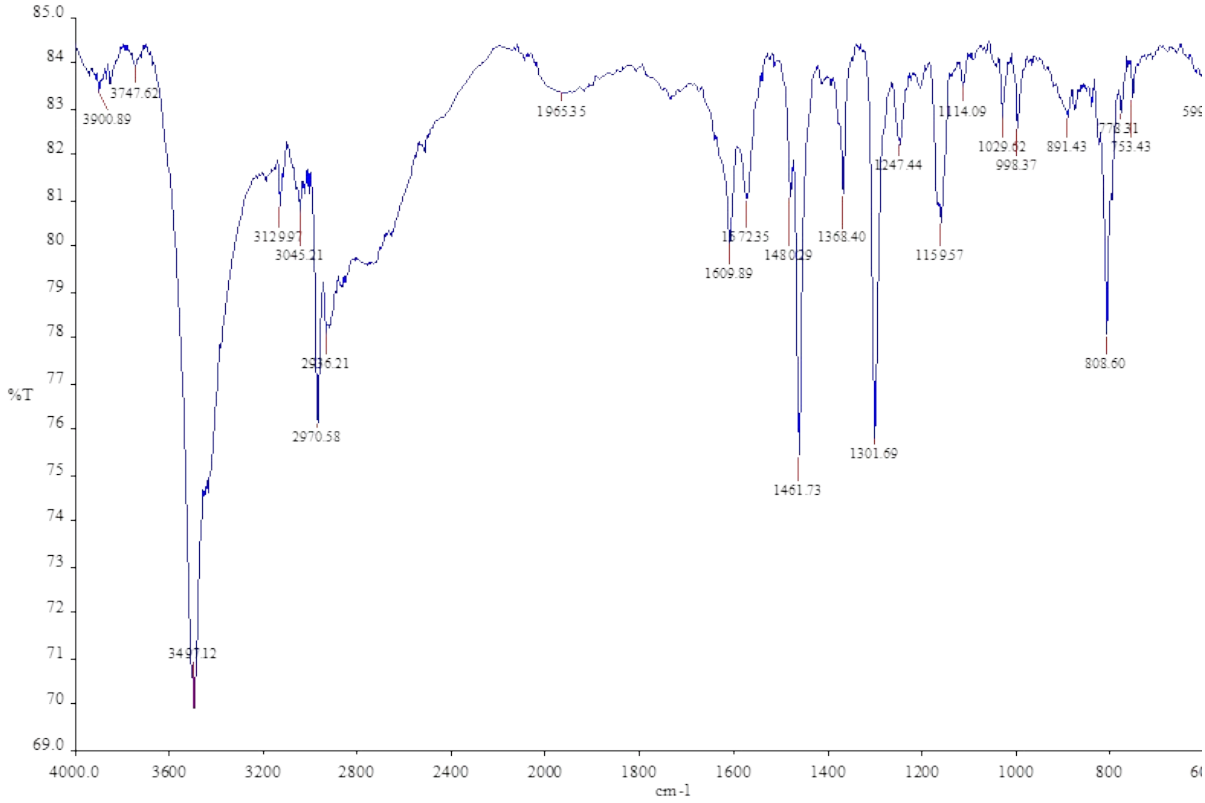

Fig. S1. FT-IR spectra of complex **1**.

A)

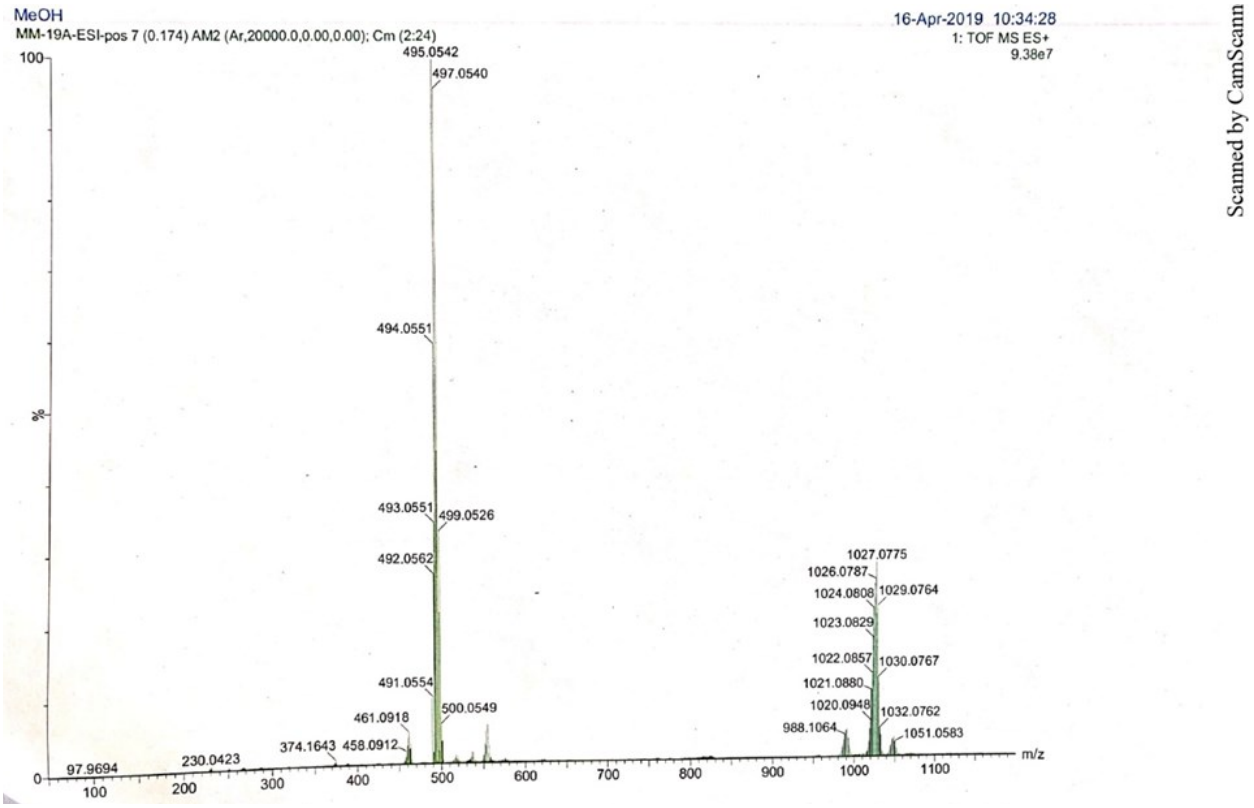

B)

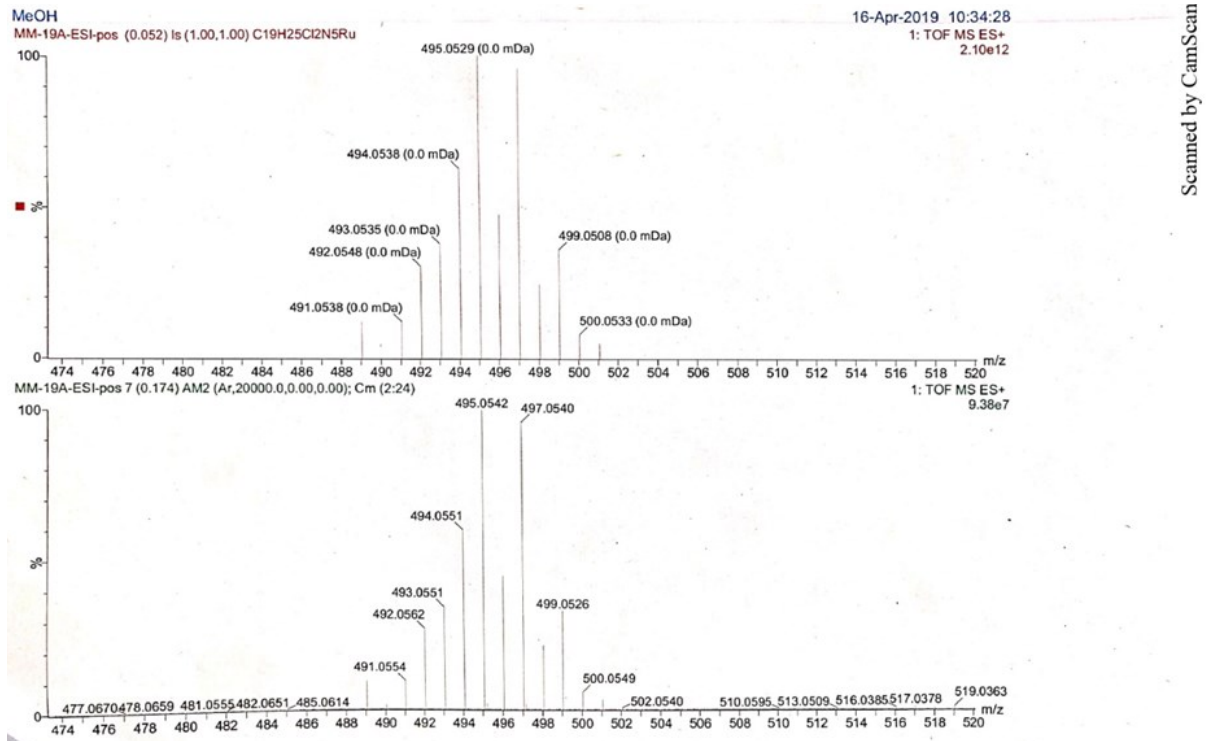

Fig. S2. ESI Q-TOF mass spectrum of the complex **1** (A) dissolved in methanol. The spectrum was acquired in the positive mode. Instrumental settings were: capillary voltage 2.8

kV, cone voltage 32 V, desolvation gas 650 L/h, desolvation temperature 350 °C and source temperature 120 °C. The isotopic distribution of the major peak from the spectrum (m/z 495.0542 in (A)) is shown in Figure (B). The theoretical and experimentally obtained isotopic distributions are shown in parallel.

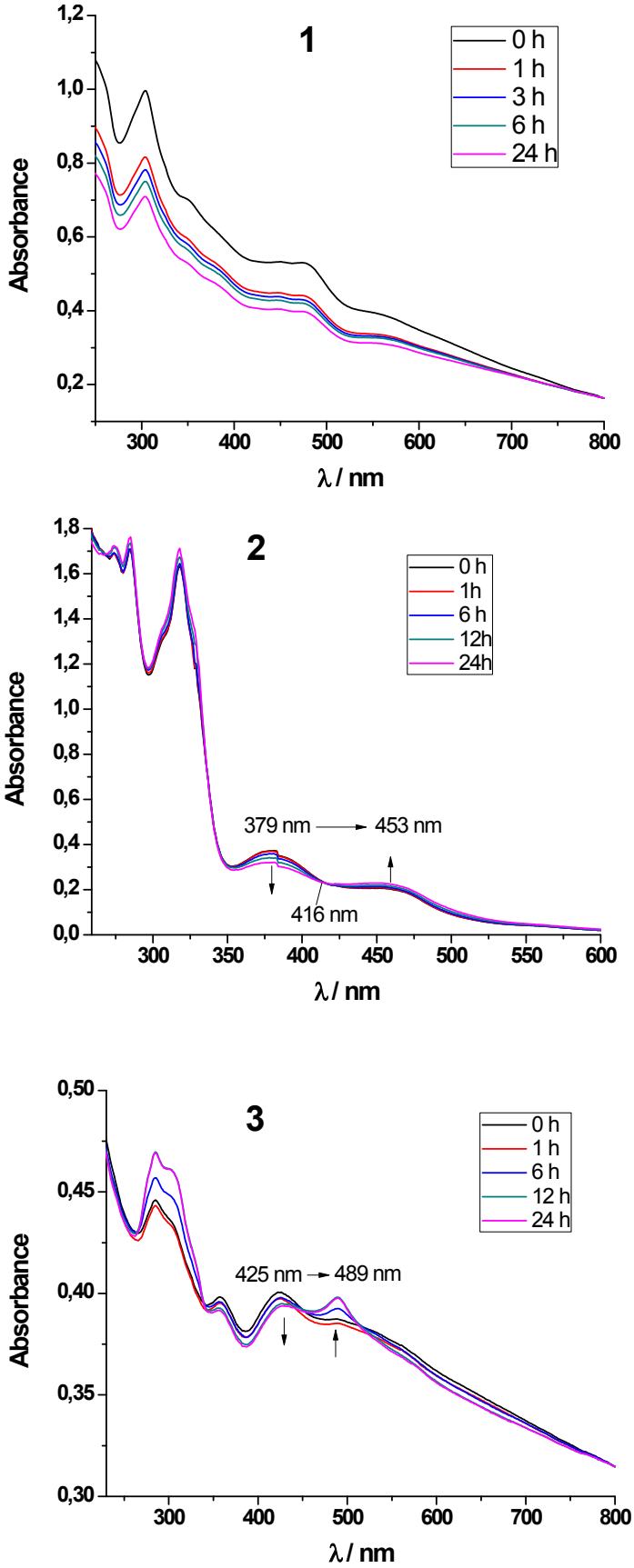

Fig. S3. UV-Vis spectra of complexes **1 – 3** in water over a 24 h period. [Ru(II)] = 1 x 10^{-4} M, T = 25 ºC.

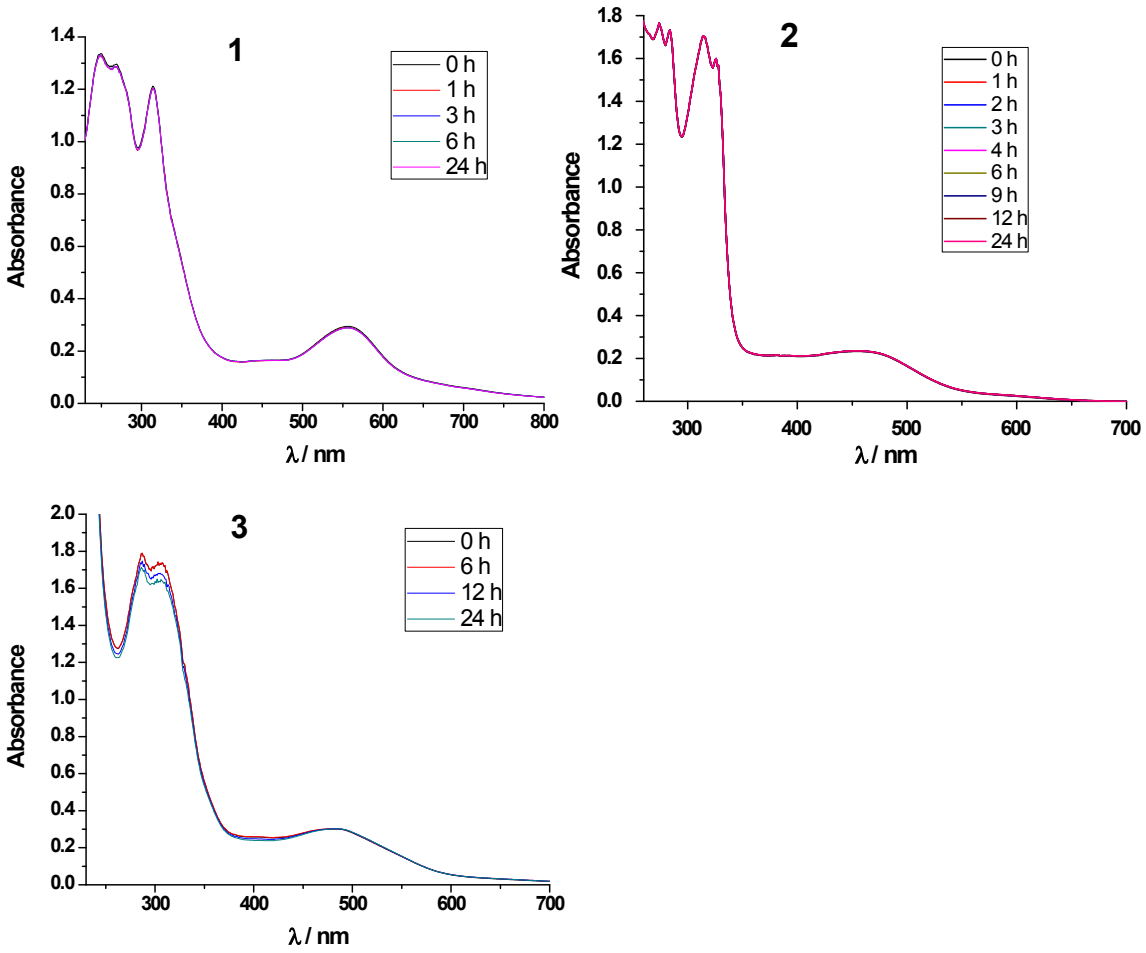

Fig. S4. UV-Vis spectra of complexes **1 – 3** in 10 mM Tris-HCl over a 24 h period. [Ru(III)] = 1 x 10^{-4} M, T = 25 ºC.

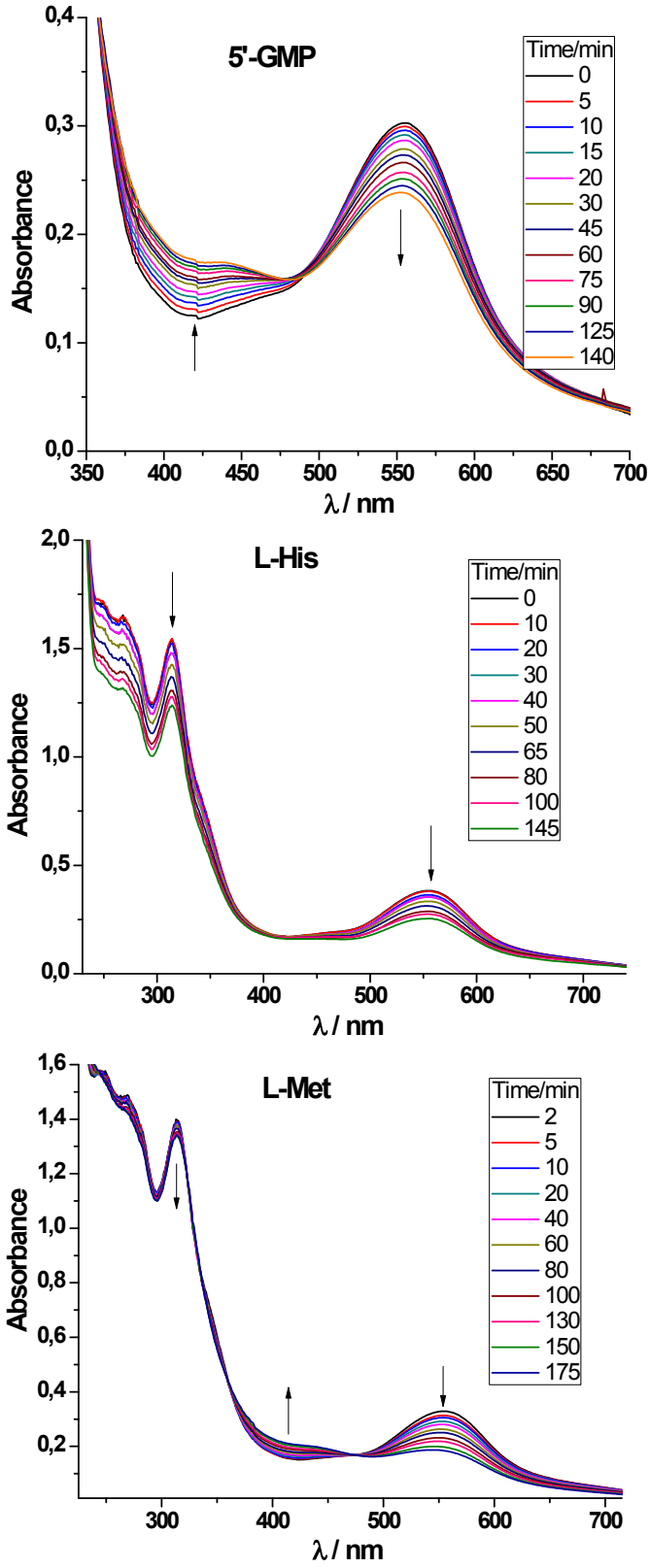

Fig. S5. Time evolution of UV-Vis spectra during the interaction of the complex **1** with 5'-GMP, L-His and L-Met in 10 mM Tris-HCl buffer (pH = 7.4) at 310 K.

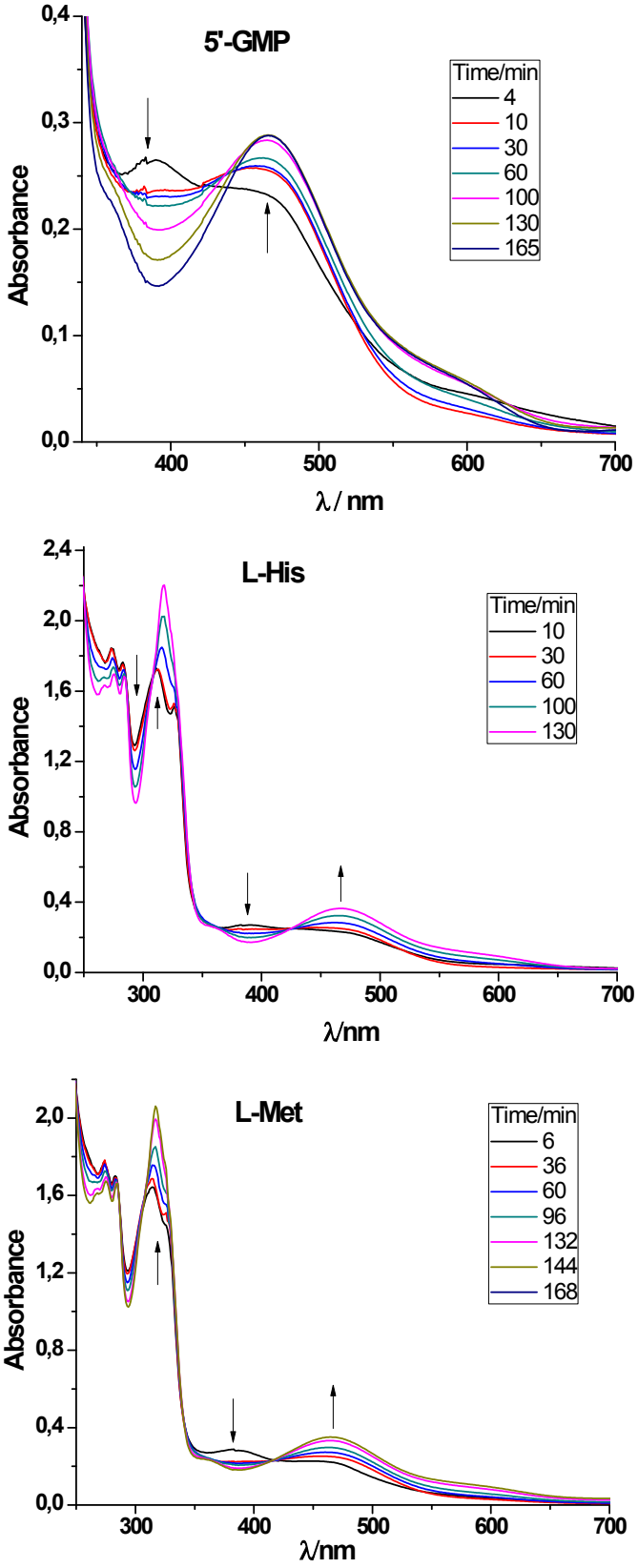

Fig. S6. Time evolution of UV-Vis spectra during the interaction of the complex **2** with 5'-GMP, L-His and L-Met in 10 mM Tris-HCl buffer (pH = 7.4) at 310 K.

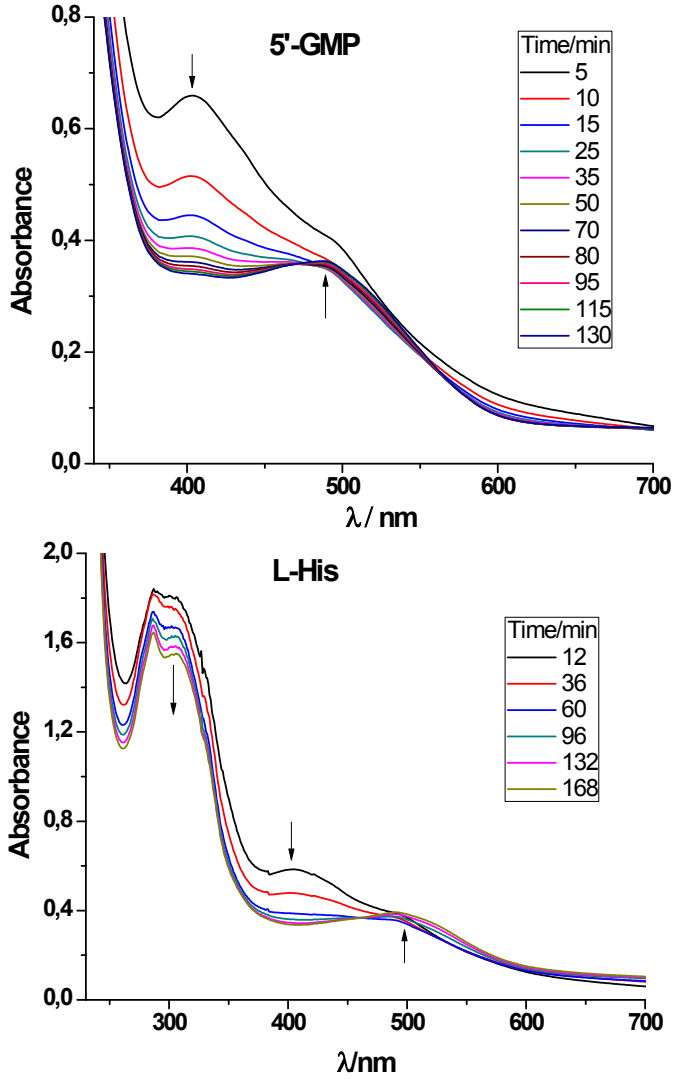

Fig. S7. Time evolution of UV-Vis spectra during the interaction of the complex **3** with 5'-GMP and L-His in 10 mM Tris-HCl buffer (pH = 7.4) at 310 K.

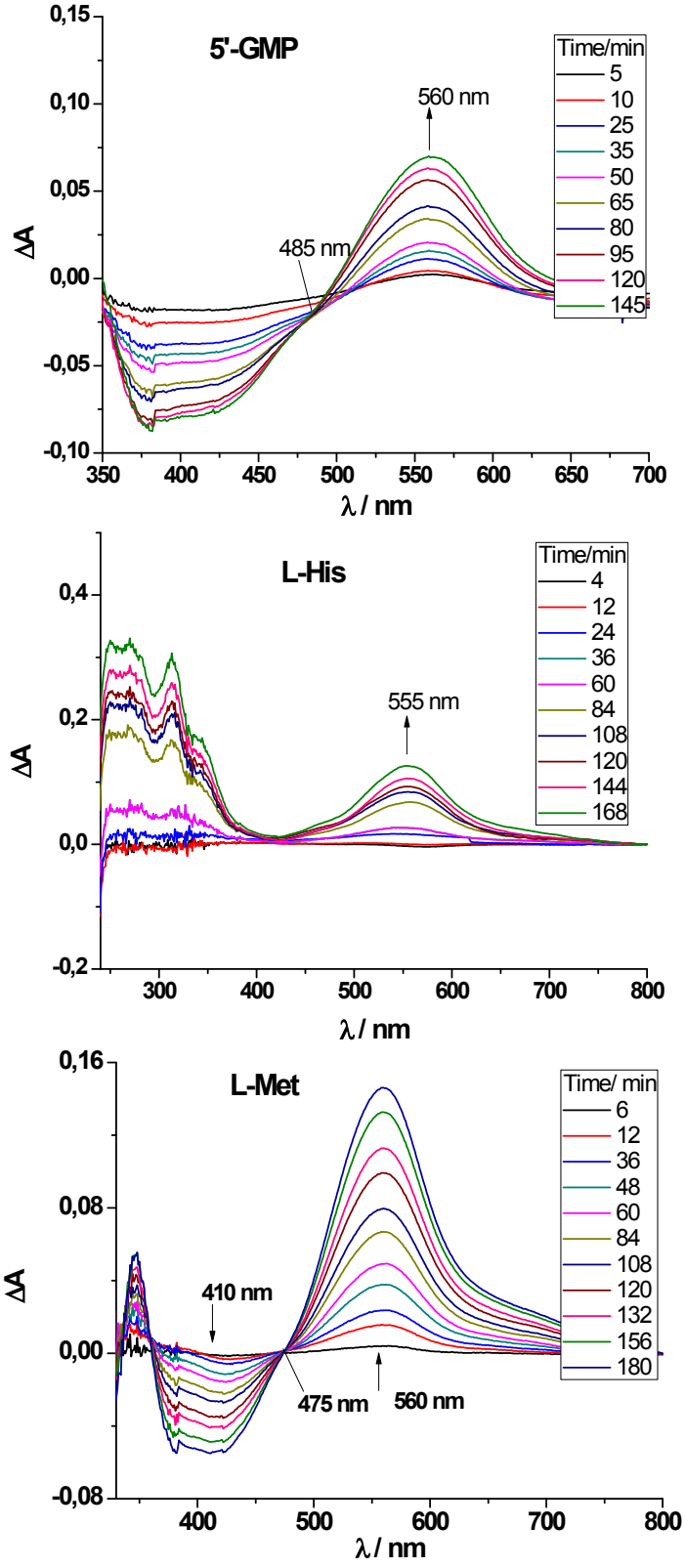

Fig. S8. Time evolution of UV-Vis difference spectra during the interaction of the complex **1** with 5'-GMP, L-His and L-Met in 10 mM Tris-HCl buffer (pH = 7.4) at 310 K. $\Delta A = A_t - A_0$, where A_t = absorbance at time t and A_0 = absorbance at the time at which the first spectrum was recorded

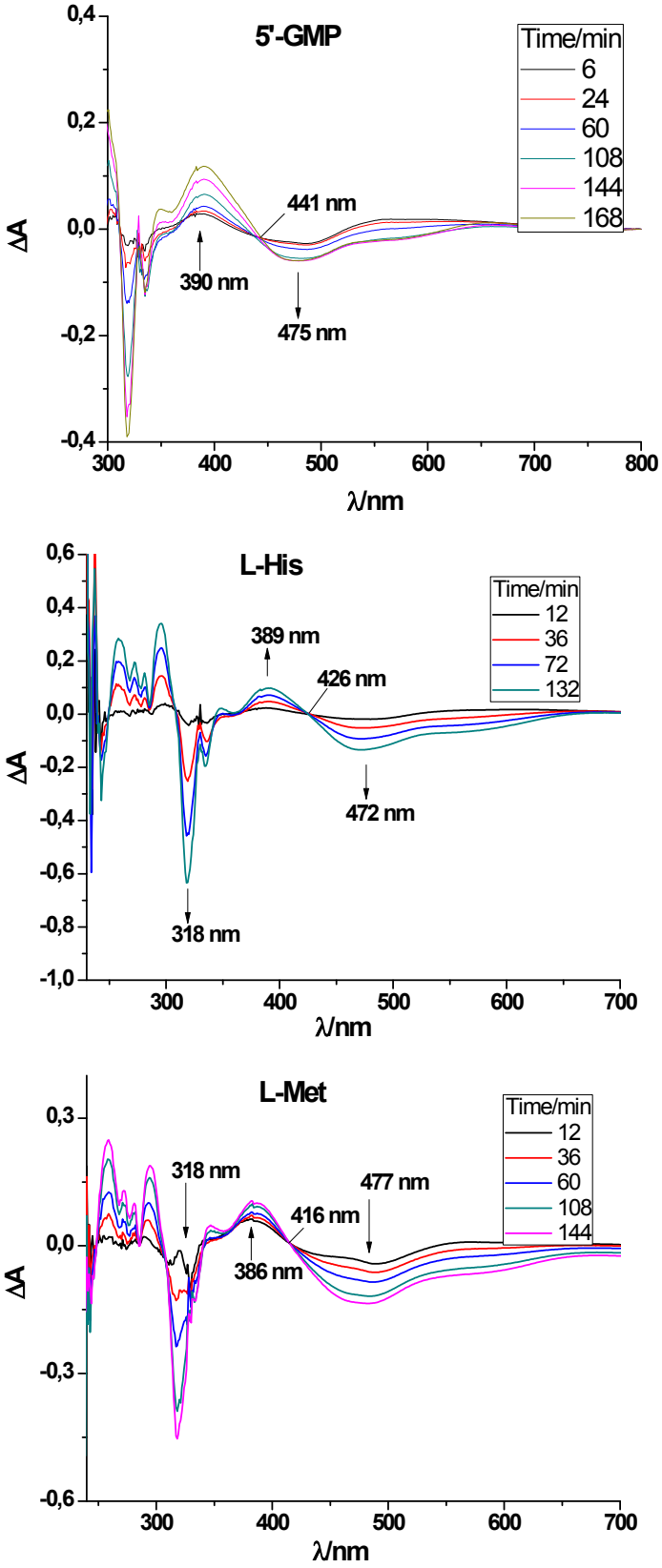

Fig. S9. Time evolution of UV-Vis difference spectra during the interaction of the complex **2** with 5'-GMP, L-His and L-Met in 10 mM Tris-HCl buffer (pH = 7.4) at 310 K. $\Delta A = A_t - A_0$,

where A_t = absorbance at time t and A_0 = absorbance at the time at which the first spectrum was recorded

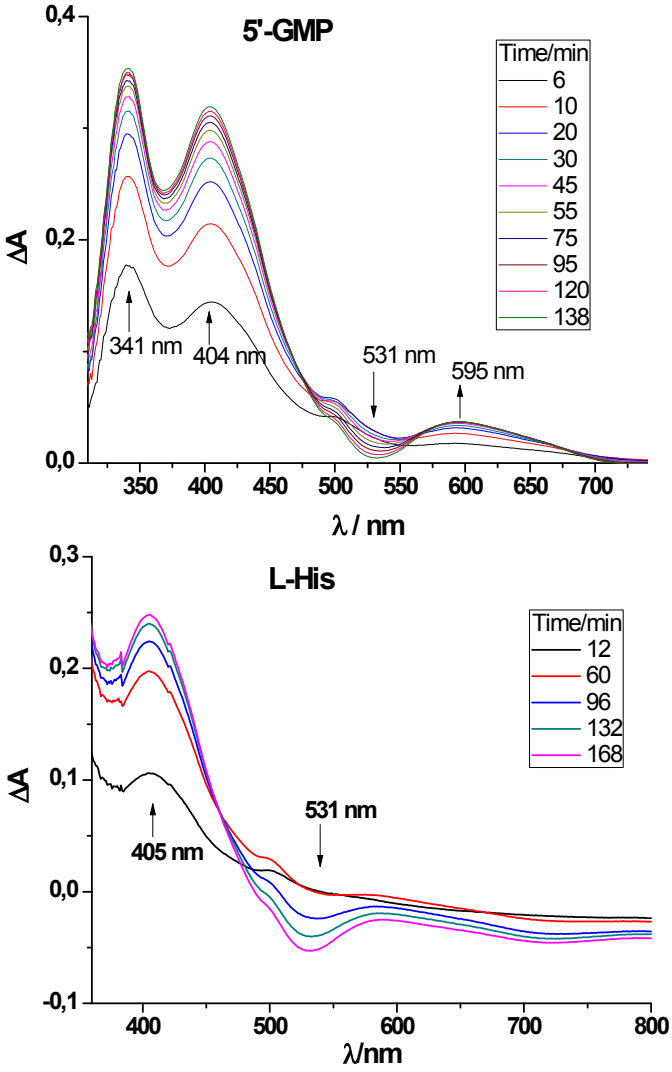

Fig. S10. Time evolution of UV-Vis difference spectra during the interaction of the complex **3** with 5'-GMP, L-His and L-Met in 10 mM Tris-HCl buffer (pH = 7.4) at 310 K. $\Delta A = A_t - A_0$, where A_t = absorbance at time t and A_0 = absorbance at the time at which the first spectrum was recorded

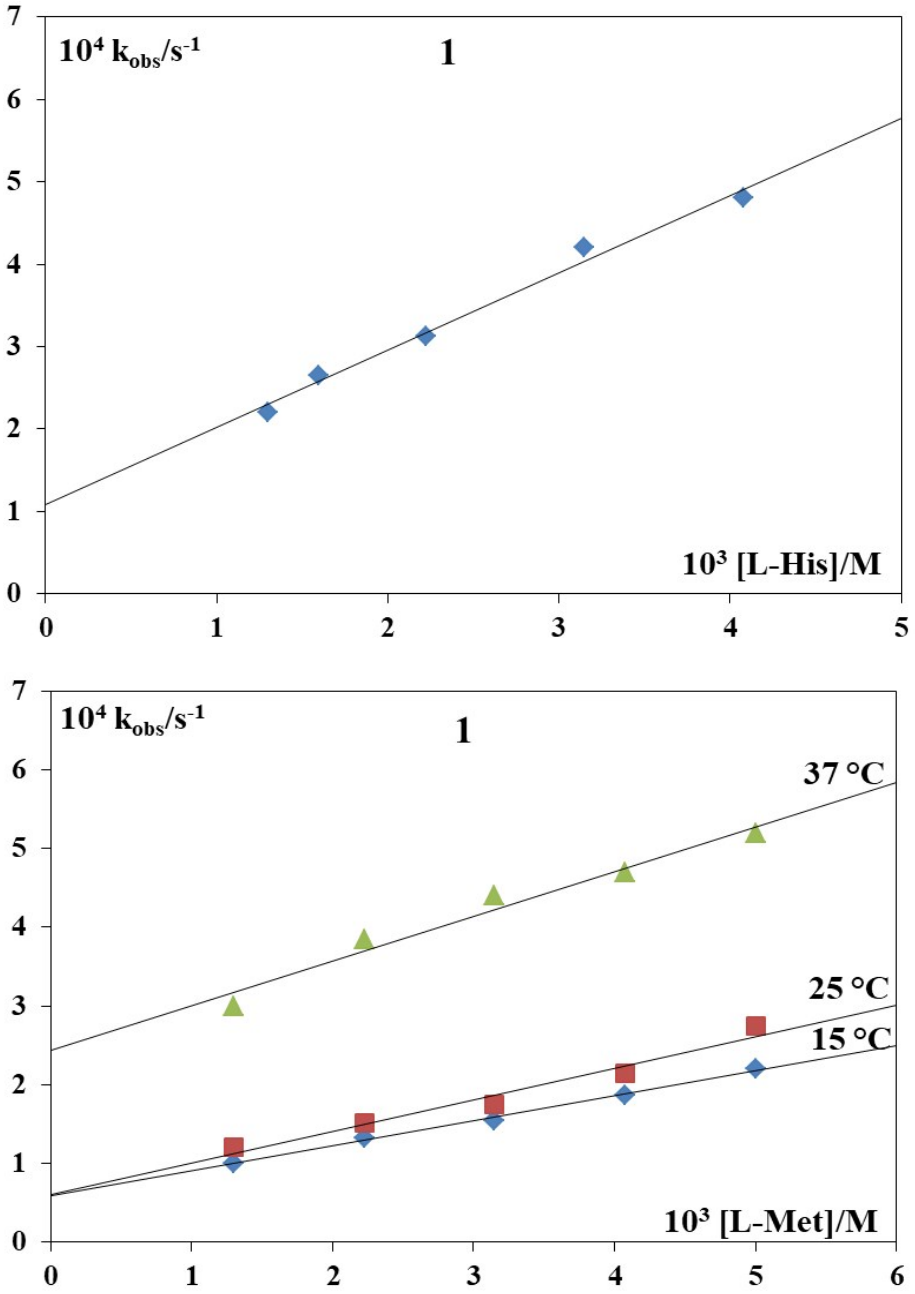

Fig. S11. *Pseudo*-first order rate constants, k_{obs}, as a function of nucleophile concentration and temperature for the substitution reaction of complex **1** with L-His and L-Met in 10 mM Tris-HCl/150 mM NaCl (pH=7.4).

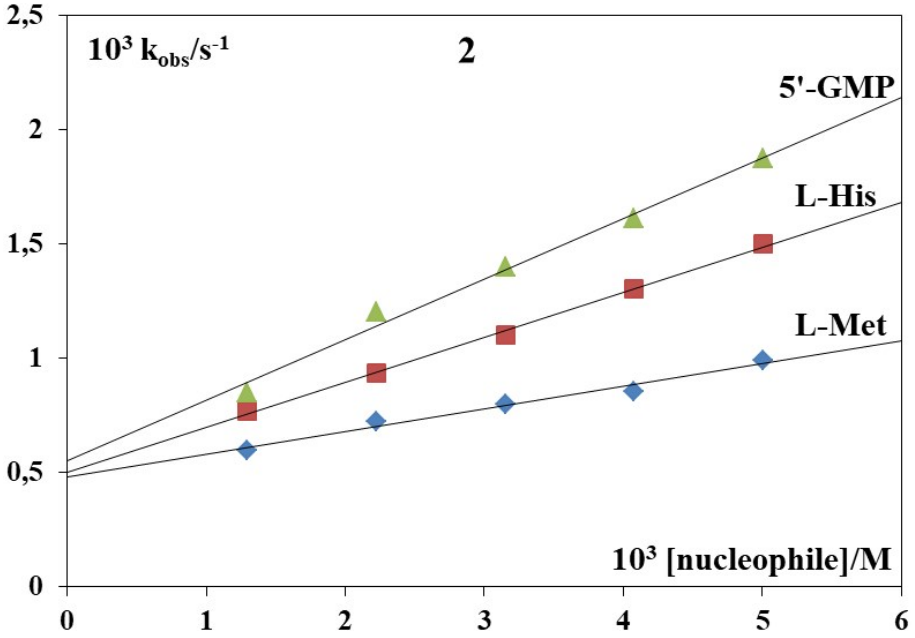

Fig. S12. *Pseudo*-first order rate constants, k_{obs}, as a function of nucleophile concentration for the substitution reaction of complex **2** with 5'-GMP, L-His and L-Met in 10 mM Tris-HCl/150 mM NaCl (pH=7.4).

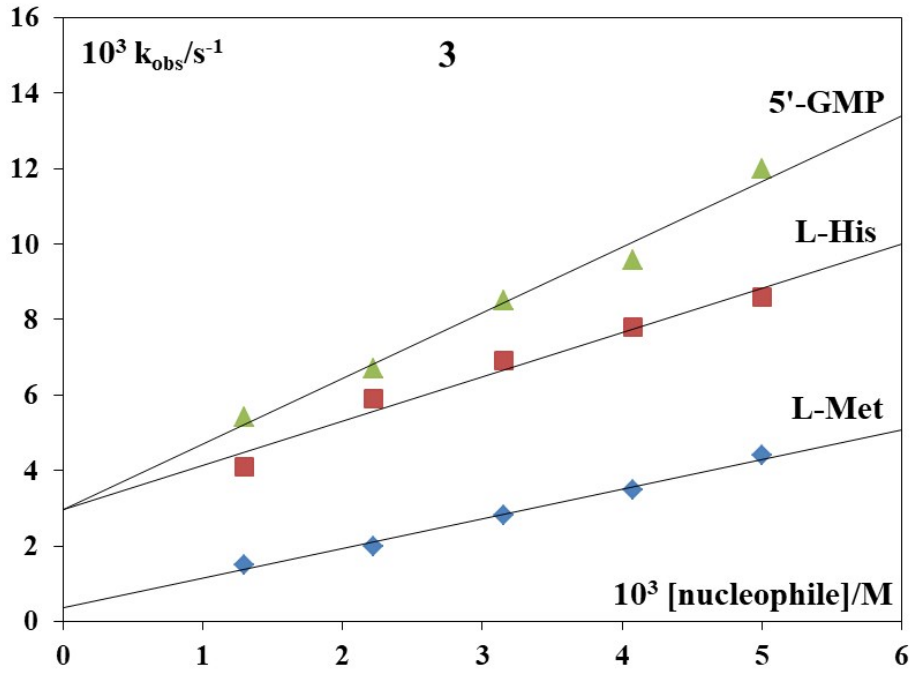

Fig. S13. *Pseudo*-first order rate constants, k_{obs}, as a function of nucleophile concentration for the substitution reaction of complex **3** with 5'-GMP, L-His and L-Met in 10 mM Tris-HCl/150 mM NaCl (pH=7.4).

,

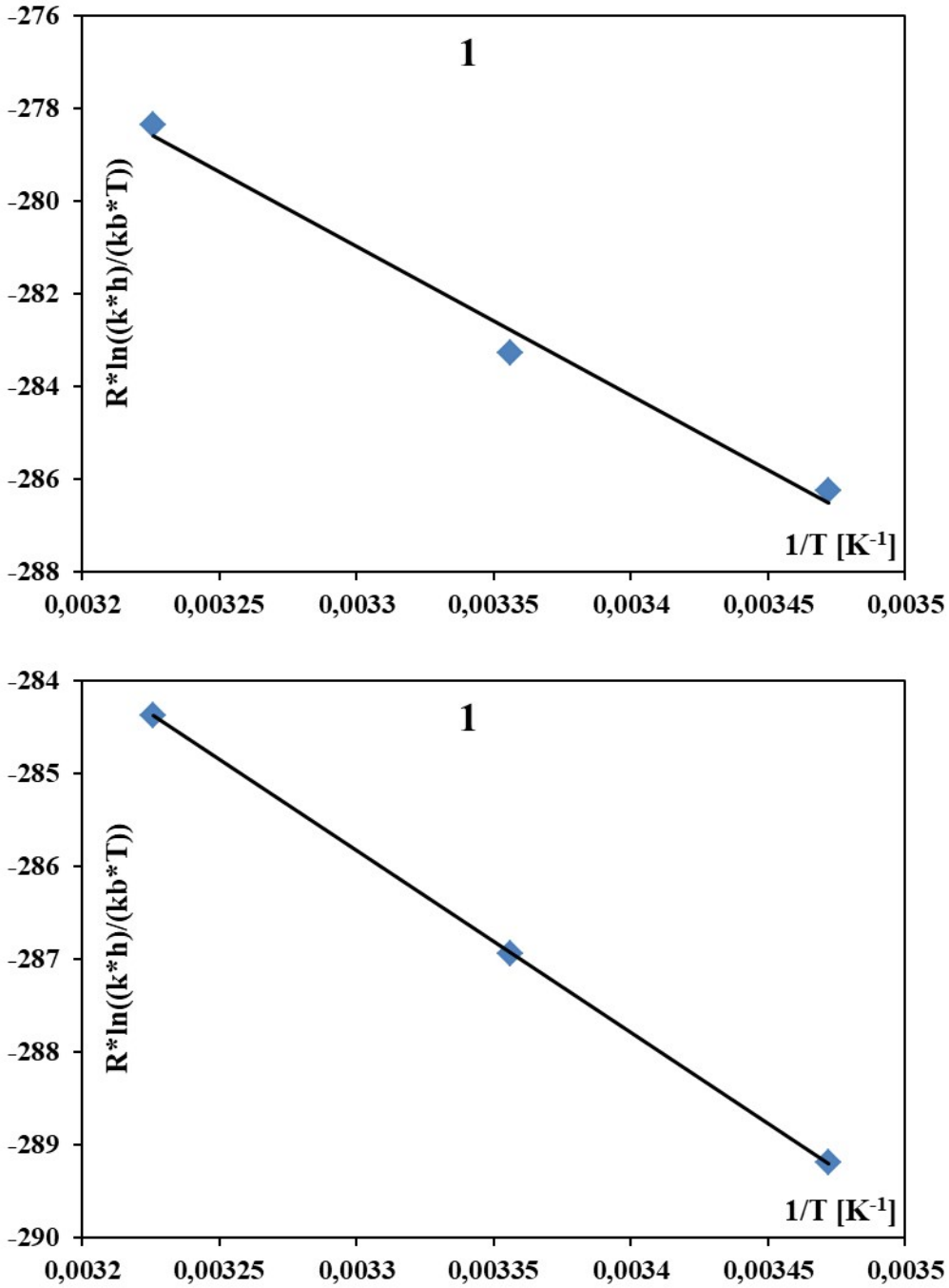

Fig. S14. Eyring plots for the reactions of complex **1** with 5'-GMP (up) and L-Met (down) in 10 mM Tris-HCl/150 mM NaCl (pH=7.4).

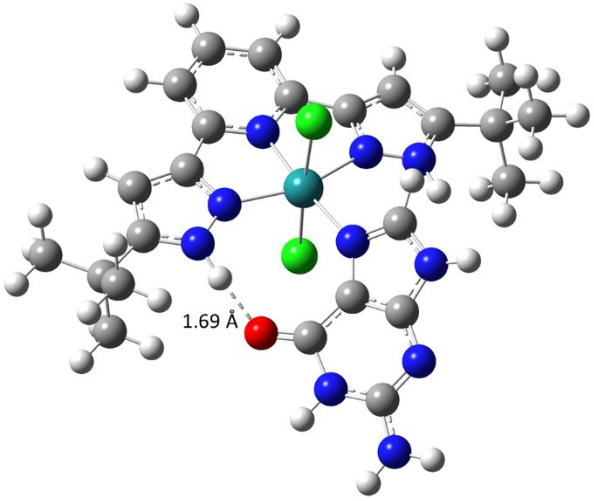

Fig. S15. Calculated (ωB97XD/def2-SVP) structure of a *trans*-[$RuCl_2(H_2L^{t\text{-}Bu})Gua]^+$ complex with selected hydrogen bond presented in angstoms.

DNA-binding studies

Calculation of DNA-binding constants

In order to compare quantitatively the binding strength of the complexes, the intrinsic binding constants K_b were determined by monitoring the changes in absorption at the MLCT band with increasing concentration of CT DNA using the following equation (S1)[S1]

$$[DNA]/(\varepsilon_A - \varepsilon_f) = [DNA]/(\varepsilon_b - \varepsilon_f) + 1/[K_b(\varepsilon_b - \varepsilon_f)] \quad (S1)$$

K_b is given by the ratio of slope to the *y* intercept in plots $[DNA]/(\varepsilon_A - \varepsilon_f)$ *versus* [DNA] (Fig. S17), where [DNA] is the concentration of DNA in base pairs, $\varepsilon_A = A_{obsd}/[complex]$, ε_f is the extinction coefficient for the unbound complex and ε_b is the extinction coefficient for the complex in the fully bound form.

Stern-Volmer equation for EB competitive studies

The relative binding of complexes to CT-DNA is described by Stern-Volmer equation (S2)[S2]:

$$I_0/I = 1 + K_{sv}[Q] \quad (S2)$$

where I_0 and I are the emission intensities in the absence and the presence of the quencher (complexes **1, 2** or **3**), respectively, [Q] is the total concentration of quencher, K_{sv} is the Stern-Volmer quenching constant, which can be obtained from the slope of the plot of I_0/I *versus* [Q] (Fig. S19).

Stern-Volmer equation for HSA quenching studies

Fluorescence quenching is described by Stern–Volmer equation:

$$I_0/I = 1 + k_q \tau_0 [Q] = 1 + K_{sv}[Q] \quad (S3)$$

where I_0 = the initial tryptophan fluorescence intensity of HSA, I = the tryptophan fluorescence intensity of HSA after the addition of the quencher, k_q = the quenching rate constants of HSA, K_{sv} = Stern-Volmer quenching constant, τ_0 = the average lifetime of HSA without the quencher, [Q] = the concentration of the quencher respectively.

$$K_{sv} = k_q \tau_0 \quad (S4)$$

and, taking as fluorescence lifetime (τ_0) of tryptophan in HSA at around 10^{-8} s, K_{sv} (M^{-1}) can be obtained by the slope of the diagram I_0/I *vs* [Q] (Stern-Volmer plots, Fig. S22), and subsequently the approximate k_q (M^{-1} s^{-1}) may be calculated.[S2]

Scatchard equation for HSA quenching studies

From Scatchard equation:

$$r/D_f = nK - rK \quad (S5)$$

where r ($r = \Delta I/I_0$) is the moles of drug bound per mole of protein and D_f is the molar concentration of free metal complex. The association binding constant K (M^{-1}) may be calculated from the slope in the Scatchard plots r/D_f *vs* r and the number of binding sites per albumin (n) is given by the ratio of *y* intercept to the slope (Scatchard plots, Fig. S23).[S3]

References

S1. A. M. Pyle, J. P. Rehmann, R. Meshoyrer, C. V. Kumar, N. J. Turro and J. K. Barton, *J. Am. Chem. Soc*., 1989, **111**, 3051-3058.

S2. R. Lakowicz and G. Weber, *Biochemistry*, 1973, **12**, 4161-4170.

S3. S. Wu, W. Yuan, H. Wang, Q. Zhang, M. Liu, K. Yu, *J. Inorg. Biochem*., 2008, **102**, 2026-2034.

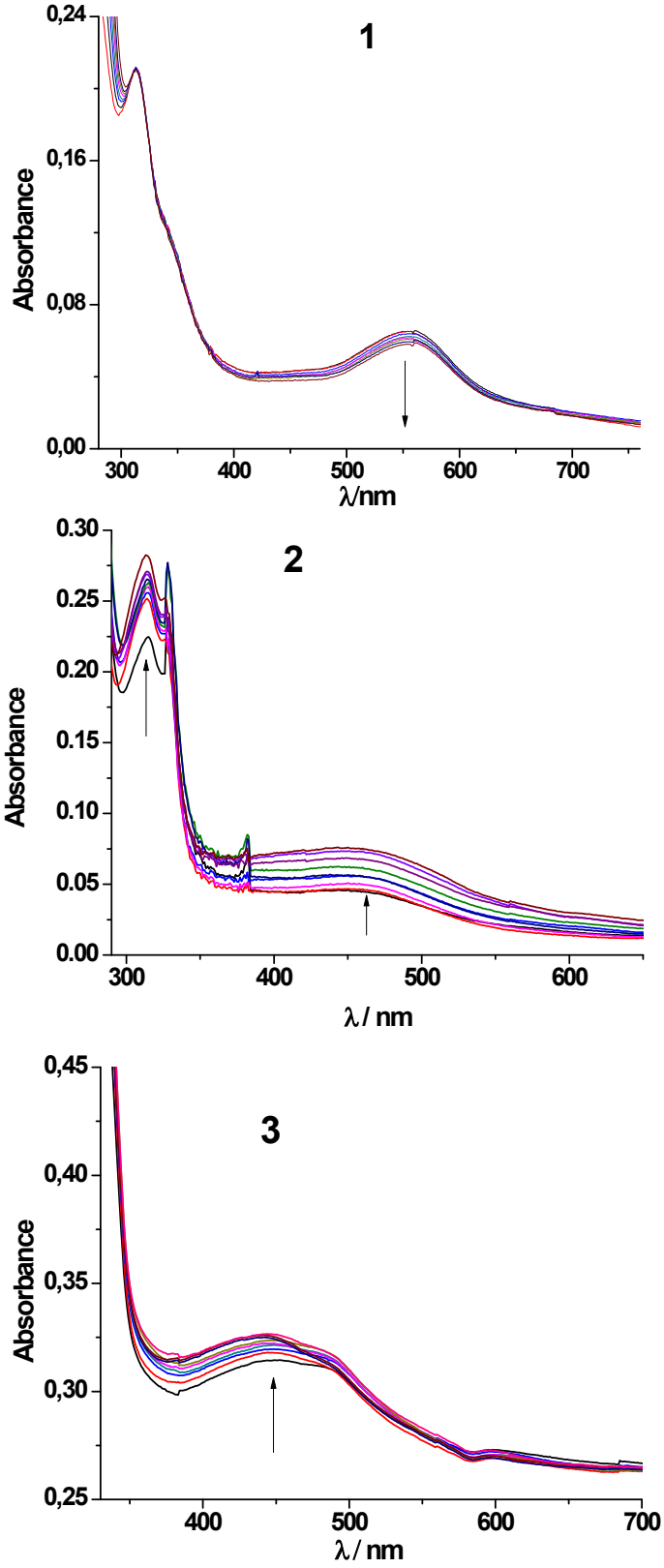

Fig. S16. Absorption spectra of complexes **1**–**3** in 10 mM Tris-HCl (150 mM NaCl, pH 7.4) upon addition of CT DNA. [Ru] = 1.30 x 10^{-5} M, [DNA] = (0.13-1.30) x 10^{-5} M. Arrows show the absorbance changing upon increasing CT DNA concentrations.

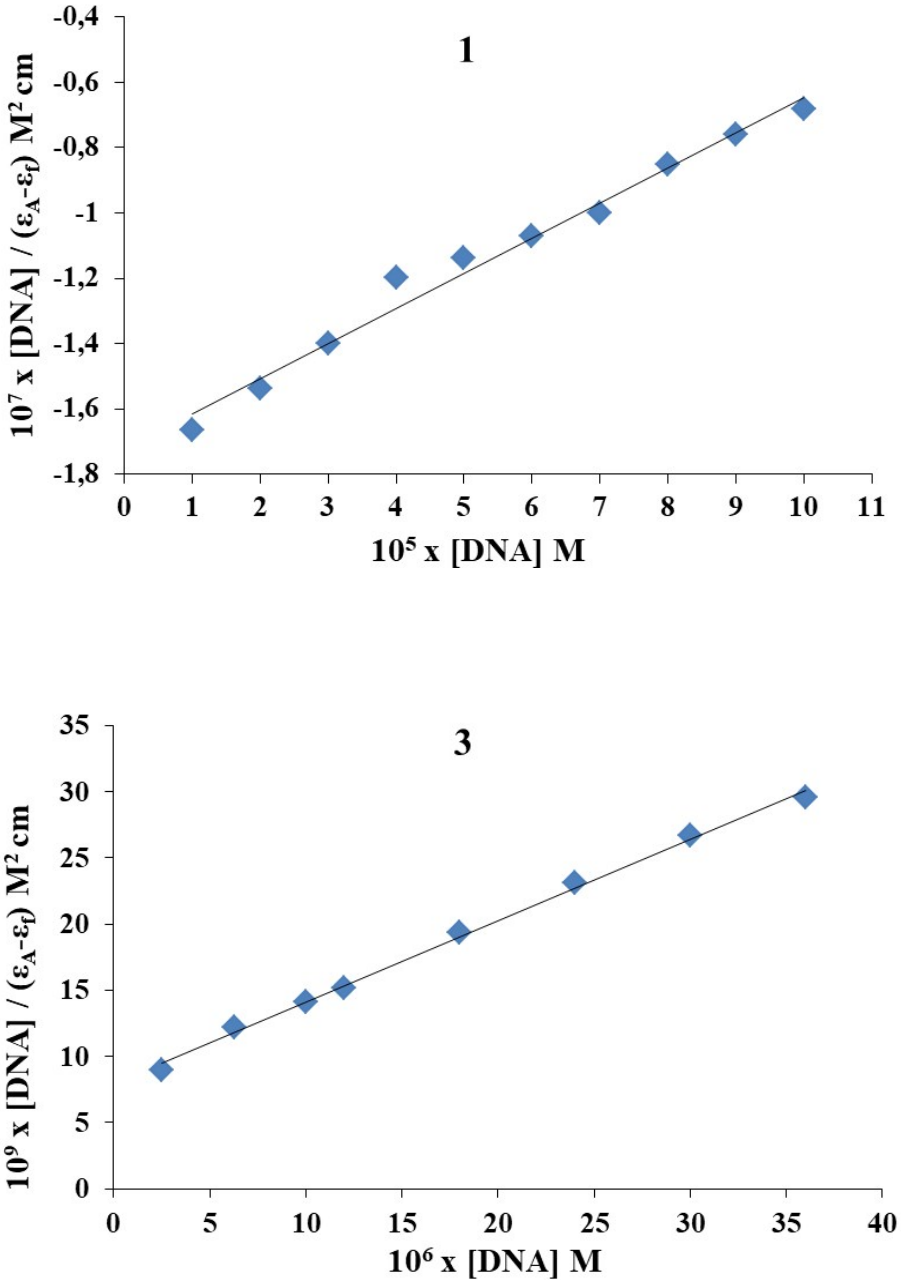

Fig. S17. Plots of [DNA]/($\varepsilon_A - \varepsilon_f$) *versus* [DNA] for the complexes **1–3**.

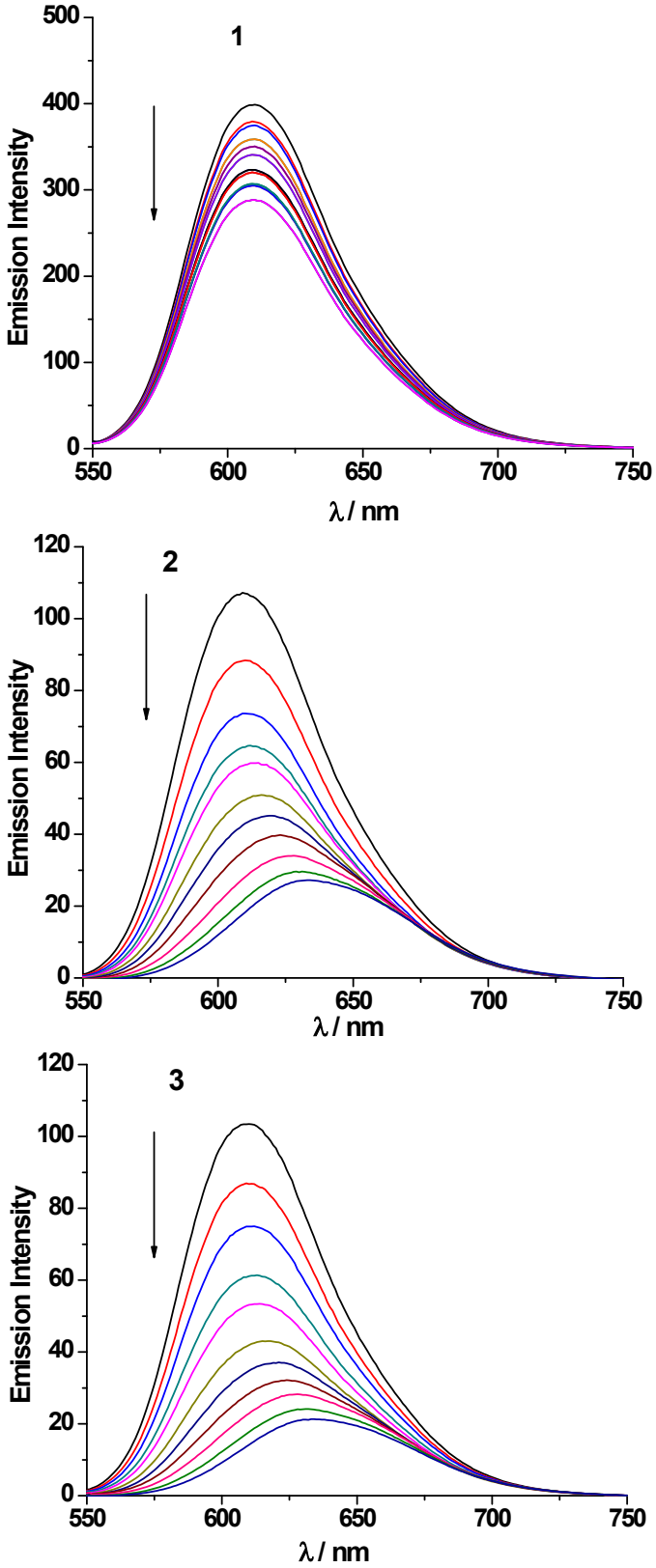

Fig. S18. Emission spectra of EB bound to DNA in the presence of complexes **1 – 3**. [EB] = 80 μM, [DNA] = 80 μM; [Ru] = 0–80 μM; λ_{ex} = 527 nm. The arrows show the intensity changes upon increased concentrations of the complexes.

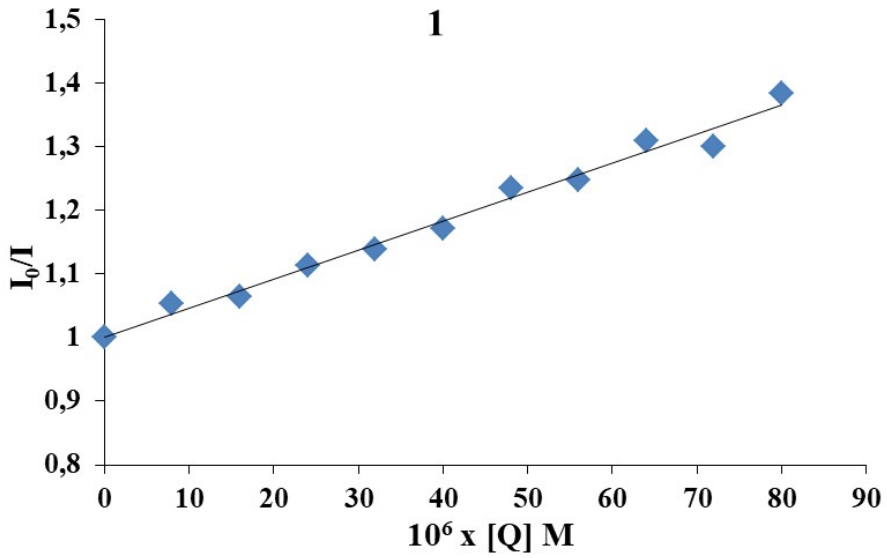
1
1,5
1,4
1,3
1,2
1,1
1
0,9
0,8
I0/I
0
10
20
30
40
50
60
70
80
90
10⁶ x [Q] M

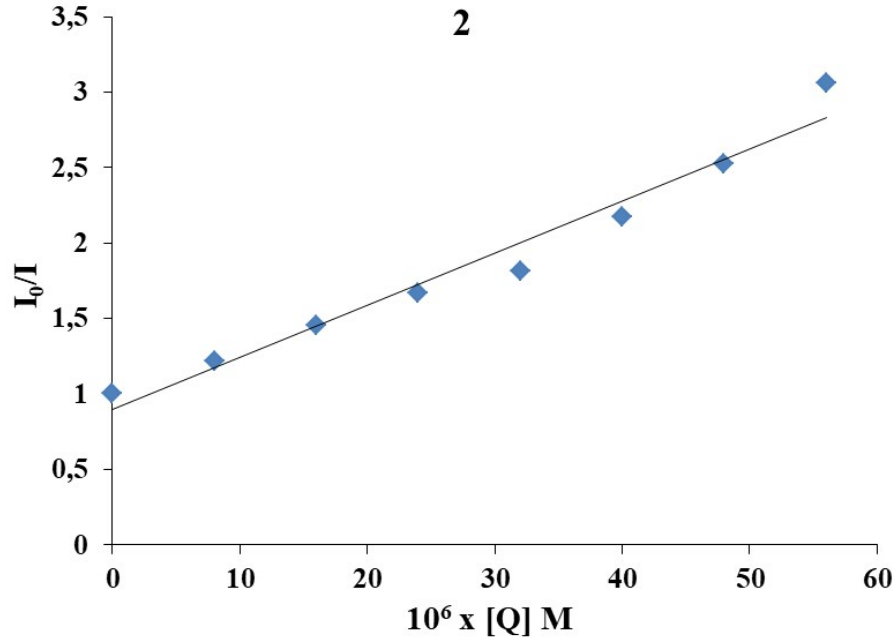
2
3,5
3
2,5
2
1,5
1
0,5
0
I0/I
0
10
20
30
40
50
60
10⁶ x [Q] M

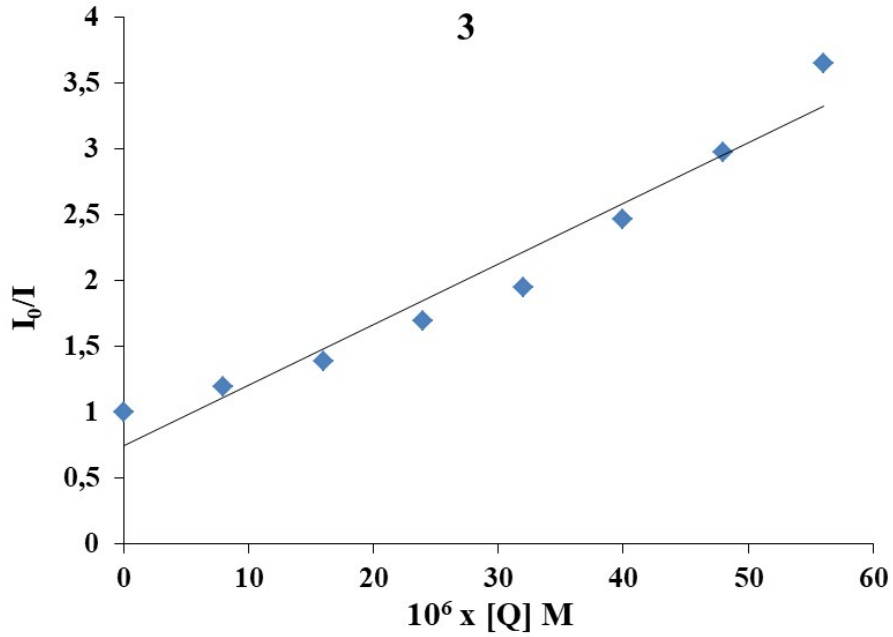

Fig. S19. Stern-Volmer quenching plot of EB-DNA for complexes **1** – **3**.

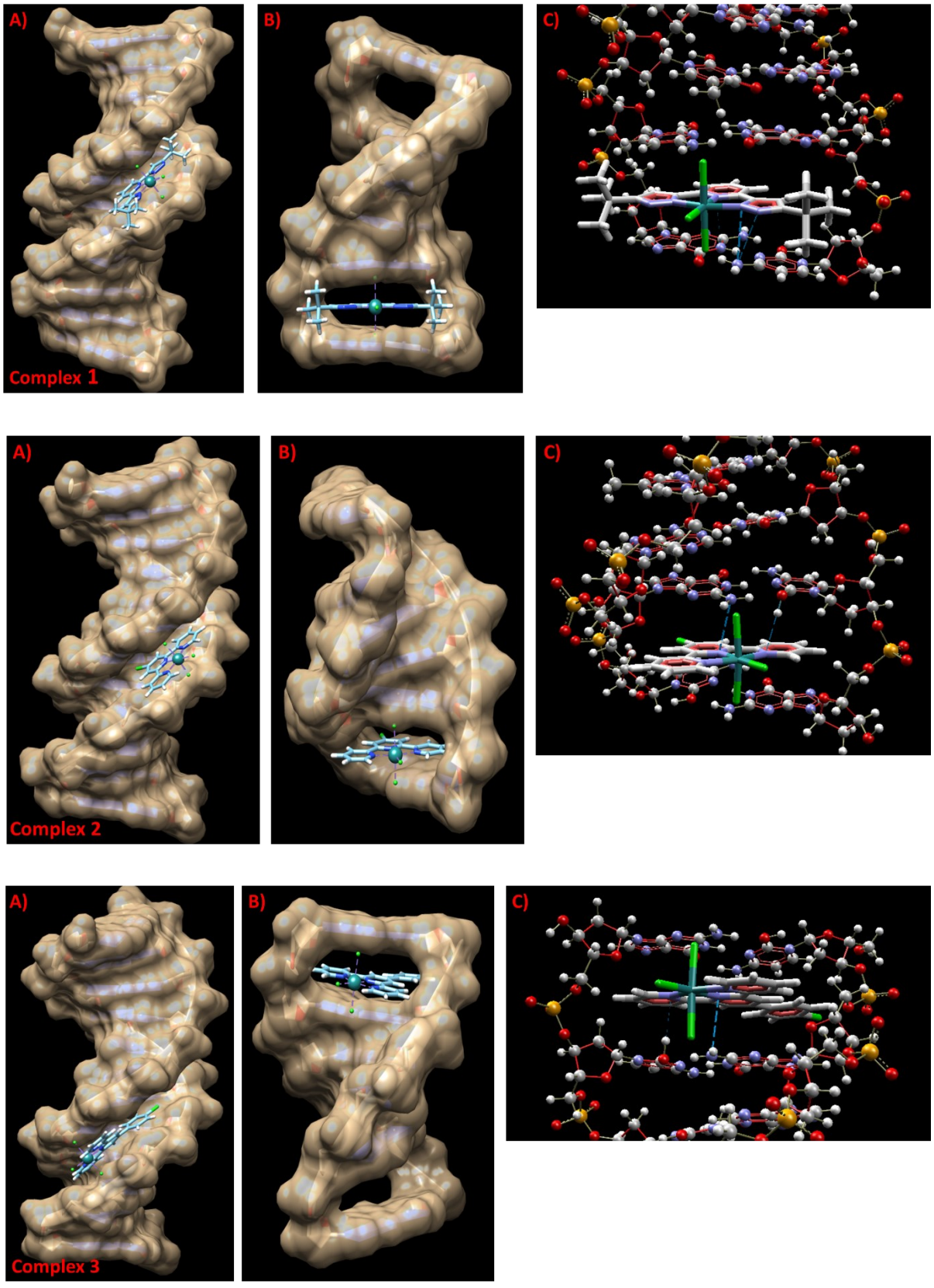

Fig. S20. Computational docking model illustrating interactions between investigated complexes **1 – 3** and A) DNA with the canonical gap, B) DNA with the intercalation gap; C)

Possibilities of formation a hydrogen bond (blue doted lines) between investigated complexes and the DNA fragments.

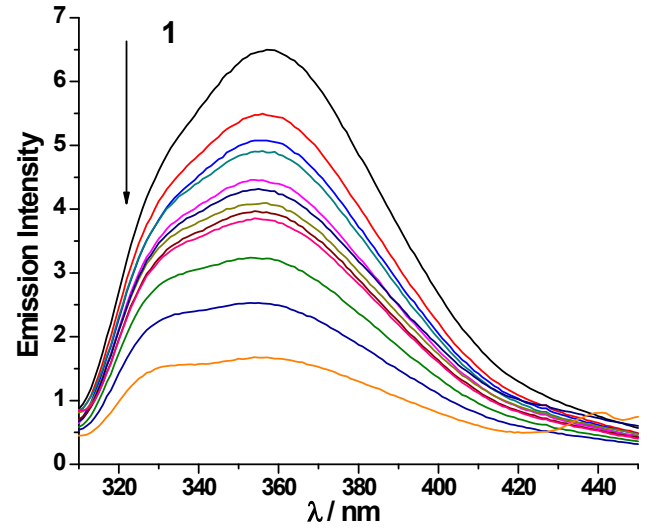

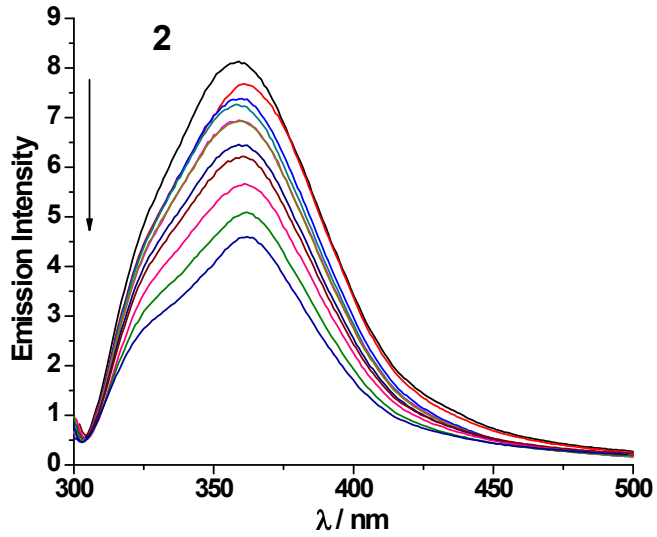

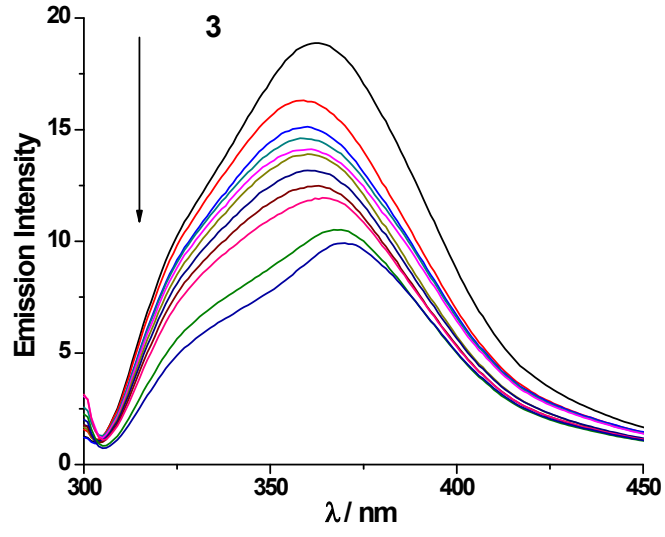

Fig. S21. Emission spectra of HSA in the presence of complexes **1 – 3**. [HSA] = [Ru] = 0–80 μM; λ_{ex} = 295 nm. The arrows show the intensity changes upon increasing concentrations of the complexes

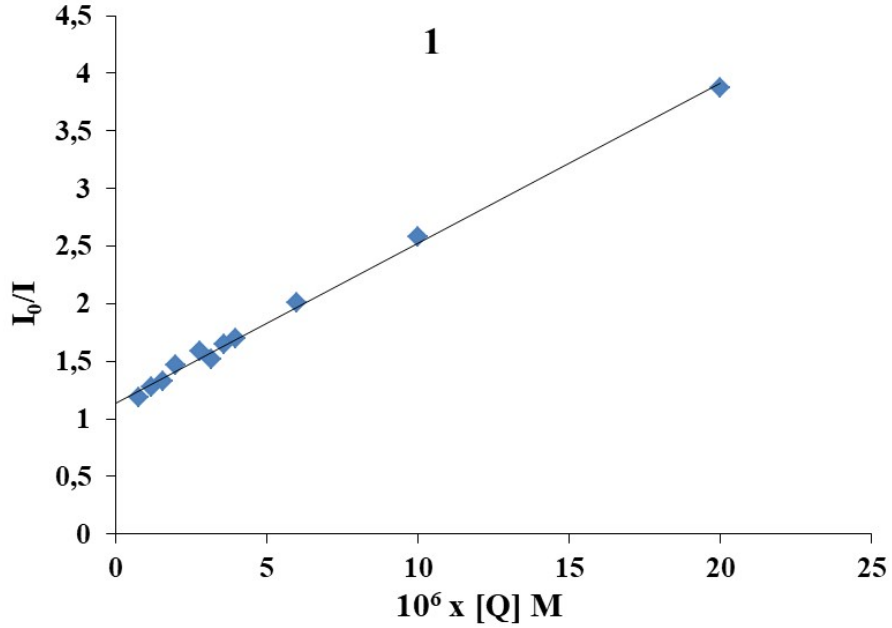

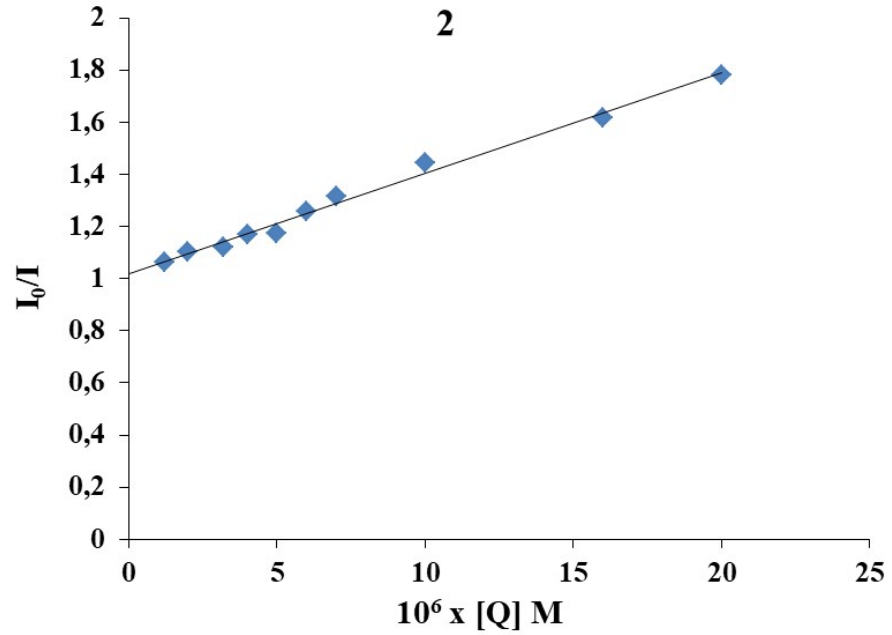

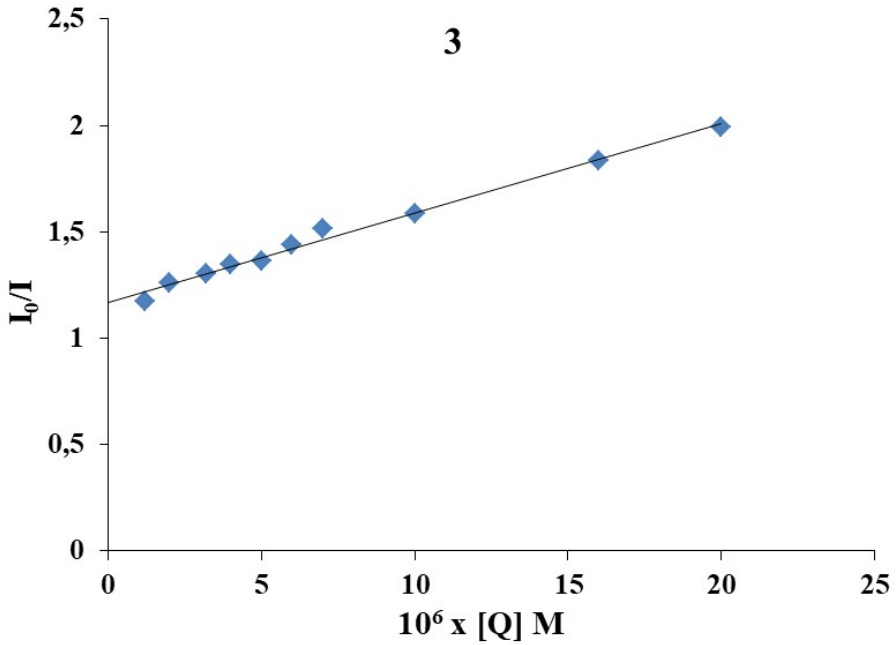

Fig. S22. Stern-Volmer quenching plot of HSA for complexes **1 – 3**.

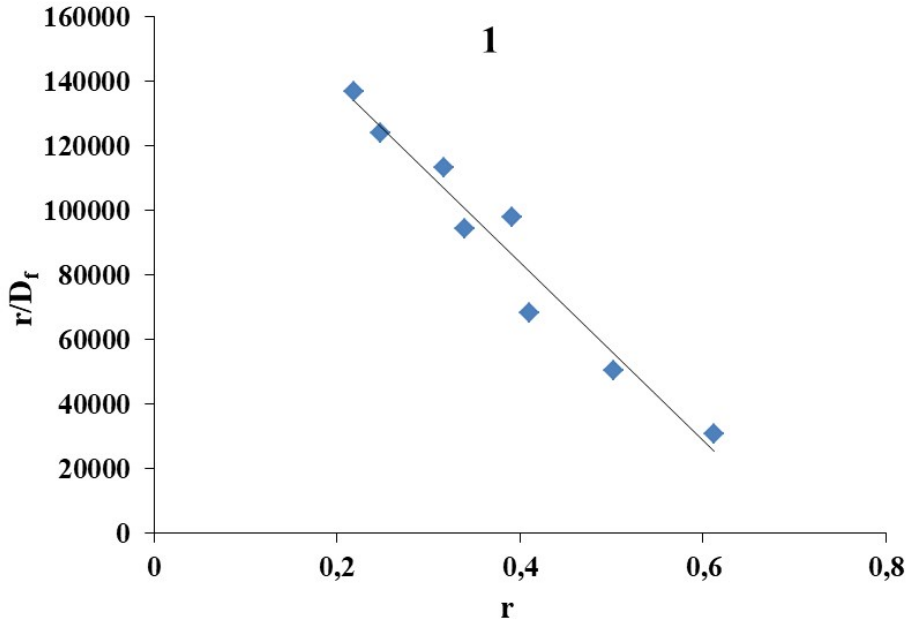
1
160000
140000
120000
100000
80000
60000
40000
20000
0
r/Df
0
0,2
0,4
0,6
0,8
r

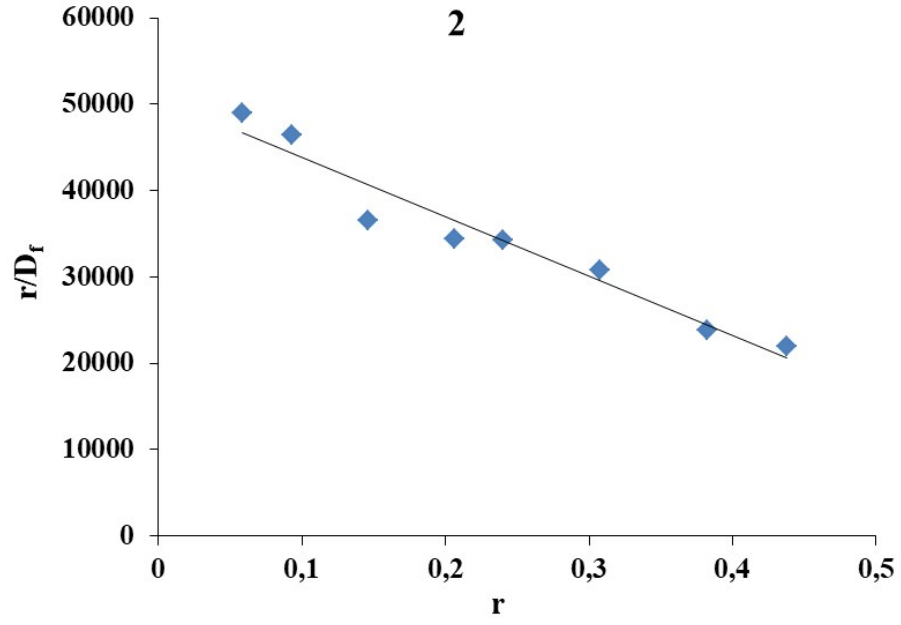
2
60000
50000
40000
30000
20000
10000
0
r/Df
0
0,1
0,2
0,3
0,4
0,5
r

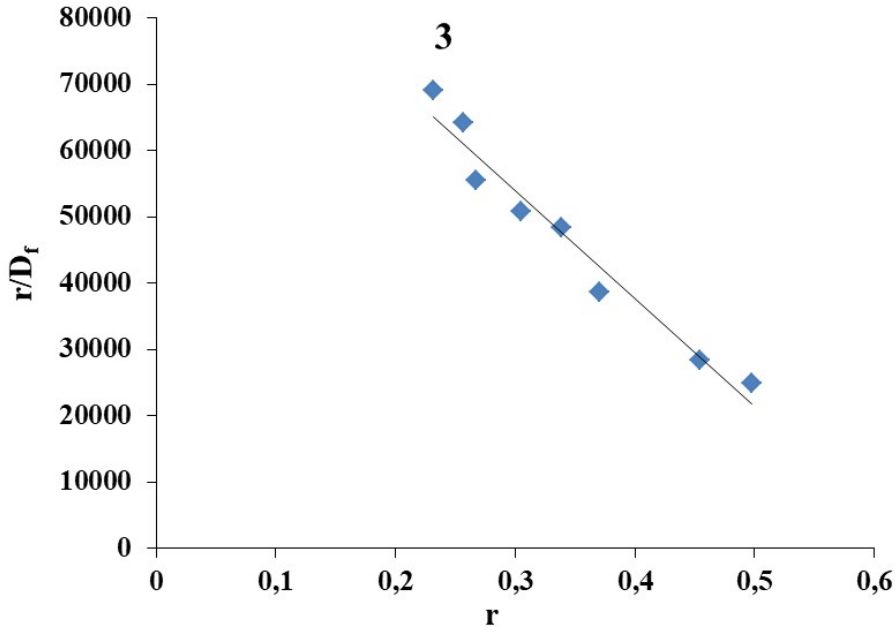

Fig. S23. Scatchard plot of HSA for complexes **1 – 3**.

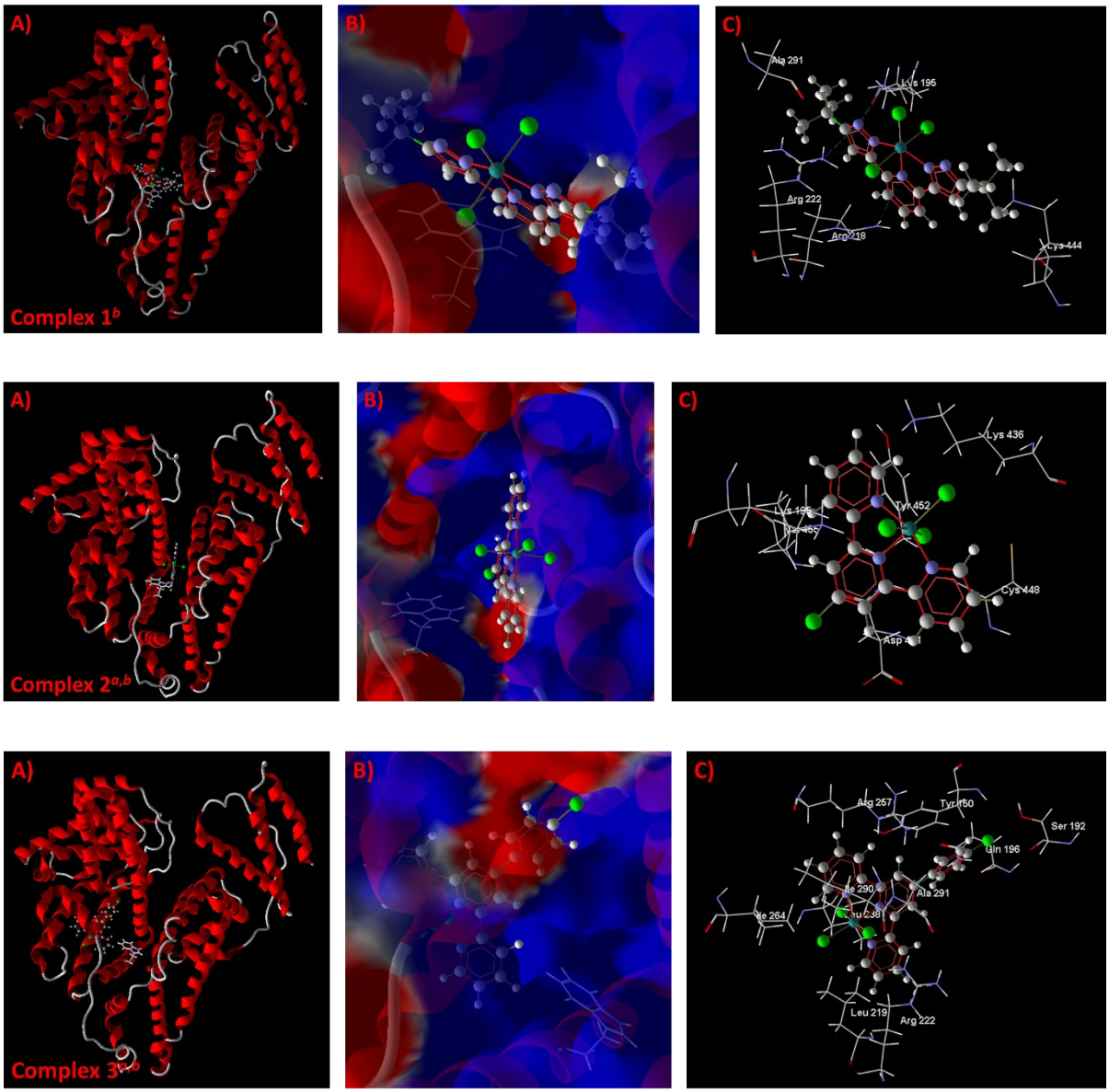

Fig. S24. Best poses with HSA for complexes **1** – **3** [a]MolDock, Docking, and Rerank scoring functions, and [b]Hbond values: A) molecular docking results illustrated regarding the HSA protein's backbone; B) complex embedded inside the active site of HSA proteins in the electrostatic view; C) binding site of investigated complexes on HSA proteins and selected amino acid residues represented by stick models. Hydrogen bonds shown in blue dotted lines.

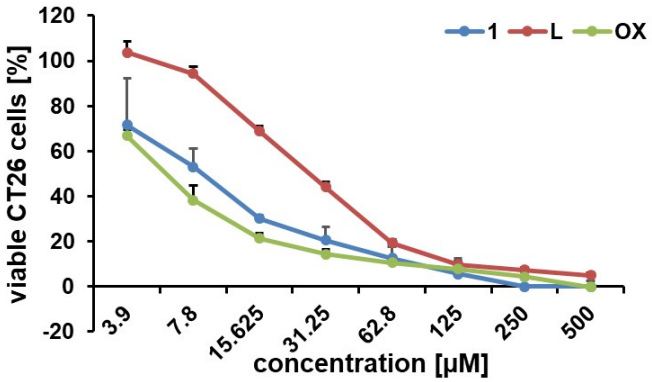

Fig. S25. The cytotoxicity of Ru(III) complex **1** against the murine colon carcinoma (CT26) cell line against different concentration after 72 h determined by MTT assay. Data are expressed as the mean±standard deviation (mean±SD).

A) B)

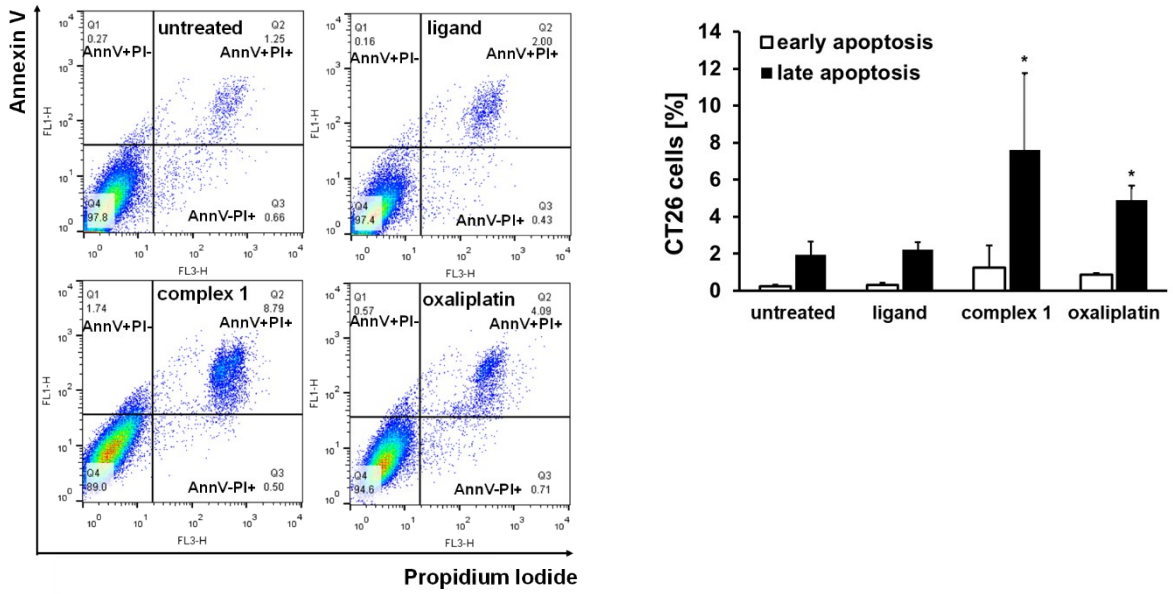

Fig. S26. Effects of ruthenium(III) complex on apoptosis of murine colon carcinoma CT26 cells. A) Representative dot plots illustrate population of viable ($AnnV^-PI^-$) early apoptotic ($AnnV^+PI^-$), late apoptotic ($AnnV^+PI^+$) and necrotic ($AnnV^-PI^+$) cells. B) Apoptosis of untreated, and **1**, bis-pyrazolylpyridine ligand and oxaliplatin treated CT26 cells were analyzed by flow cytometry using Annexin V-FITC and PI double staining. The data are presented as means ± SD of a three independent experiment, *$p < 0.05$ indicate difference between treated and untreated cells.

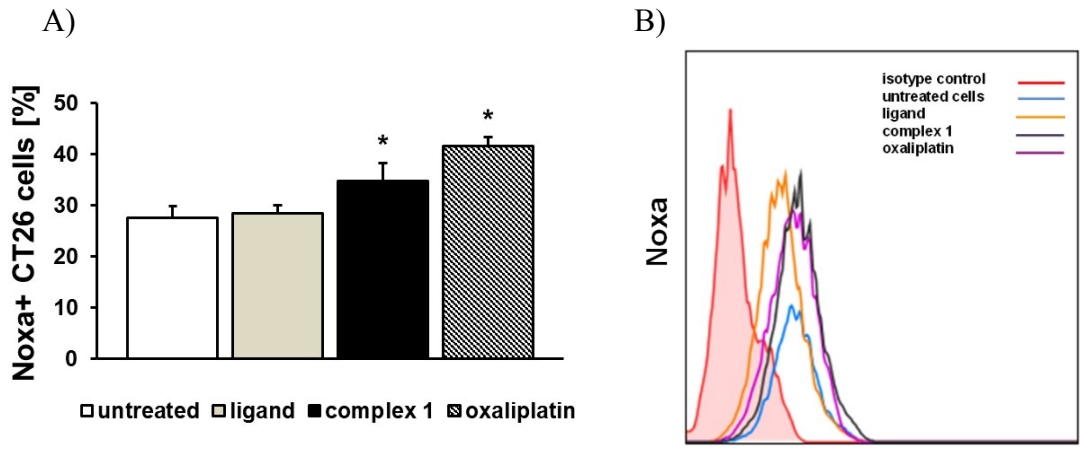

Fig. S27. Complex **1** showed weak expression of Noxa protein in CT26 cells (34.87%) compared to untreated cells (27.60%). A) Percentage of Noxa positive CT26 cells exposed to **1**, bis-pyrazolylpyridine ligand or oxaliplatin (IC_{50} value) for 24 h determined by flow cytometry presented as the mean + SD from three independent experiments. Data were analyzed with Student's *t* test: $*p < 0.05$. B) Representative histogram of Noxa expression (mean fluorescence intensity, MFI) on CT26 cells (untreated and complex **1**, bis-pyrazolylpyridine ligand or oxaliplatin treated).

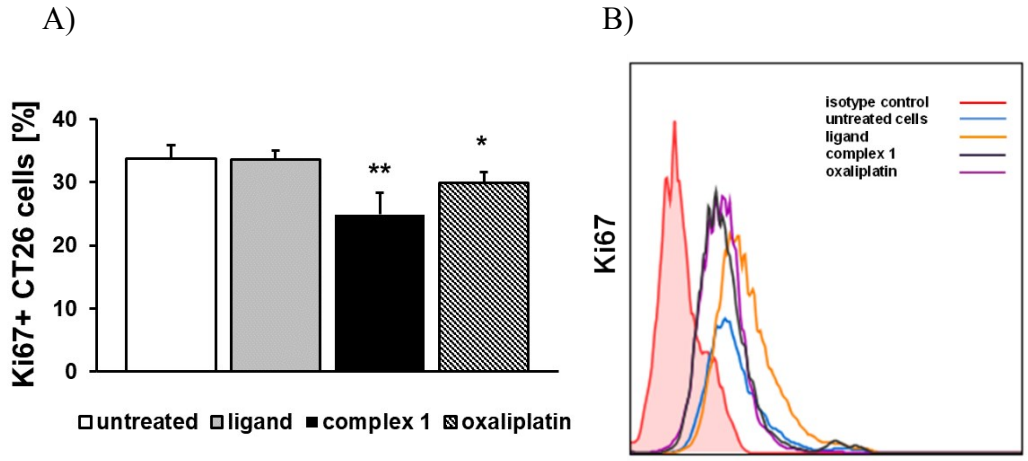

Fig. S28. Ruthenium complex **1** reduces the expression of Ki67 in CT26 cells. A) Percentage of Ki67 positive CT26 cells exposed to **1**, bis-pyrazolylpyridine ligand or oxaliplatin (IC_{50} value) for 24 h determined by flow cytometry presented as the mean + SD from three independent experiments. Data were analyzed with Student's *t* test: $*p < 0.05$, $**p < 0.01$. B) Representative histogram of Ki67 expression (mean fluorescence intensity, MFI) on CT26 cells (untreated and complex **1**, bis-pyrazolylpyridine ligand or oxaliplatin treated).

Ruthenium(III) complex 1 is well tolerated

In the present study, **1** was administered intravenously at the effective dose (10 mg/kg body weight) to evaluate the toxicological impact on treated mice. The toxicity was assessed by measuring alanine (ALT) and aspartate transaminases (AST), urea and creatinine in the serum of experimental BALB/c mice on the 21st day after the application of **1**. The results indicated that **1** in that dose was toxic to cancer cells and safe on liver and kidney cells (Fig. S29). There was no significant difference in the values of AST, ALT, urea and creatinine in the serum of **1**-treated mice compared to the control group (Fig. S29). The increased survival of **1** treated tumour bearing mice, significant reduction of colon cancer volume and weight (Figure 8), the lower incidence of metastases and the lower surface of the lung tissue affected by the metastases (Figure 9) in mice treated with **1**, significant cytotoxicity toward CT26 cells (Figure S25), with no significant hepato- and nephro-toxicity (Figure S29), suggest selective toxicity of **1** toward tumor cells.

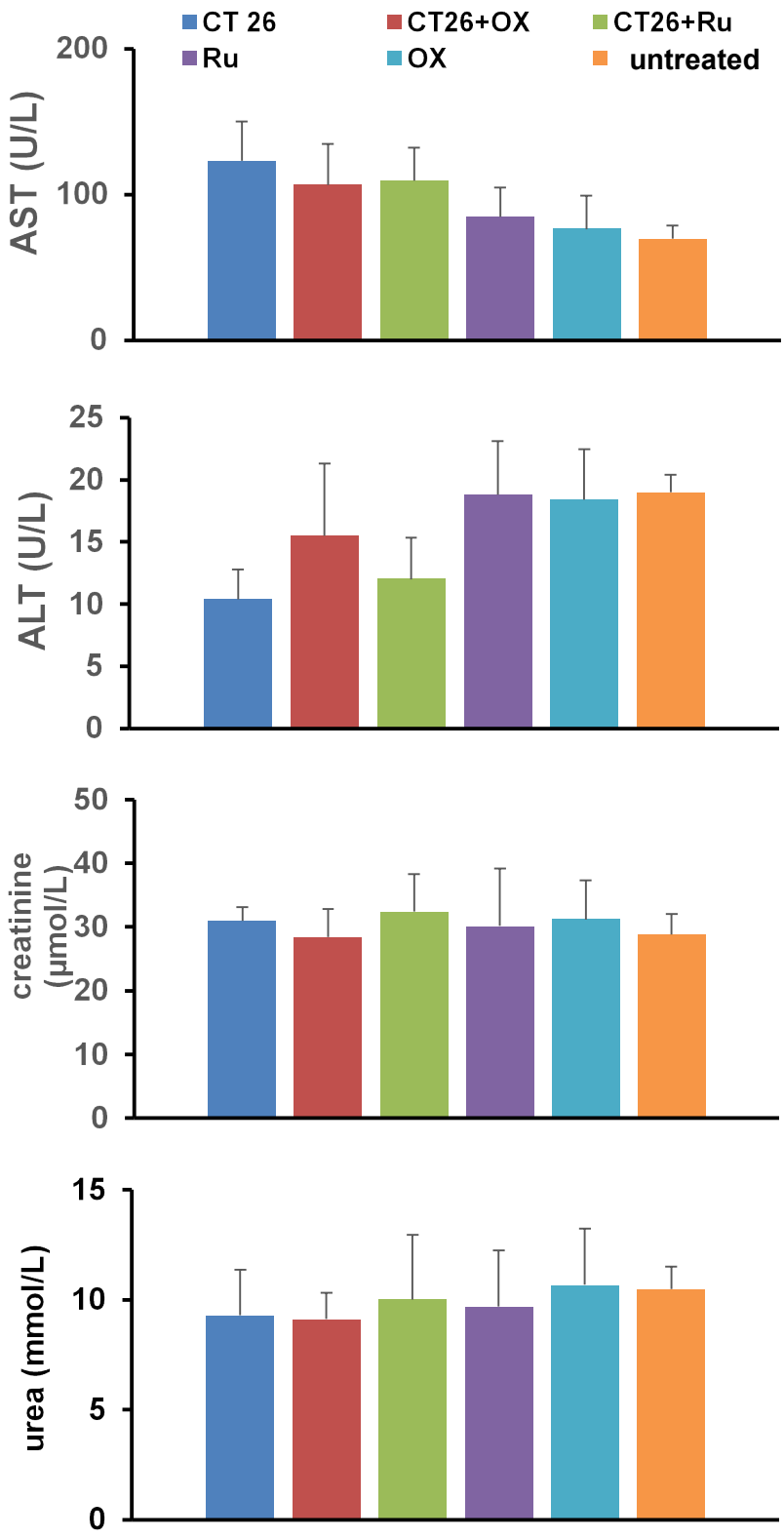

Fig. S29. Evaluation of systemic toxicity caused by i.p. application of ruthenium(III) complex 1. Concentration of urea, creatinine, ALT, and AST in the serum of tumor-bearing and mice without inoculated tumor cells, after treatment with 1 or oxaliplatin. The data are expressed as mean ± SD and statistical significance was determined by Student's t test.

Table S1. Observed *pseudo*-first order rate constants as a function of complex concentration and temperature for the reaction between complex [Ru(H_2L^{tBu})Cl_3] (**1**) and 5'-GMP (**L**) in 10 mM Tris buffer (150 mM NaCl, pH = 7.4).

t (ºC)	$C_{\mathbf{L}}$ [10^{-3} M]	k_{obs} [10^{-4} s^{-1}]
15.0	5.00	2.92(2)
	4.10	2.40(3)
	3.15	2.07(2)
	2.20	1.84(3)
	1.30	1.25(3)
25.0	5.00	3.80(3)
	4.10	3.02(3)
	3.15	2.42(2)
	2.20	2.09(3)
	1.30	1.58(3)
37.0	5.00	6.00(3)
	4.10	5.03(2)
	3.15	4.02(3)
	2.20	3.00(3)
	1.30	2.20(3)

Table S2. Observed *pseudo*-first order rate constants as a function of complex concentration and temperature for the reaction between complex [Ru(H_2L^{tBu})Cl_3] (**1**) and L-Met (**L**) in 10 mM Tris buffer (150 mM NaCl, pH = 7.4).

t (ºC)	$C_{\mathbf{L}}$ [10^{-3} M]	k_{obs} [10^{-4} s^{-1}]
15.0	5.00	2.20(2)
	4.10	1.86(3)
	3.15	1.55(2)
	2.20	1.32(3)
	1.30	1.00(3)
25.0	5.00	2.74(3)
	4.10	2.15(3)
	3.15	1.75(2)
	2.20	1.52(3)
	1.30	1.20(3)
37.0	5.00	5.20(3)
	4.10	4.70(2)
	3.15	4.40(3)
	2.20	3.84(3)
	1.30	3.30(3)

Table S3. Observed *pseudo*-first order rate constants as a function of complex concentration and temperature for the reaction between complex [Ru(H_2L^{tBu})Cl_3] (**1**) and L-His (**L**) in 10 mM Tris buffer (150 mM NaCl, pH = 7.4).

t ºC	C_L [10^{-3} M]	k_{obs} [10^{-4} s^{-1}]
37	4.10	4.80(3)
	3.15	4.20(2)
	2.20	3.12(3)
	1.60	2.65(3)
	1.30	2.20(3)

Table S4. Observed *pseudo*-first order rate constants as a function of complex concentration and temperature for the reaction between complex [Ru(Cl-tpy)Cl_3] (**2**) and 5'-GMP (**L**) in 10 mM Tris buffer (150 mM NaCl, pH = 7.4).

t ºC	C_L [10^{-3} M]	k_{obs} [10^{-3} s^{-1}]
37.0	5.00	1.87(2)
	4.10	1.61(3)
	3.15	1.40(2)
	2.20	1.20(3)
	1.30	0.85(3)

Table S5. Observed *pseudo*-first order rate constants as a function of complex concentration and temperature for the reaction between complex [Ru(Cl-tpy)Cl_3] (**2**) and L-His (**L**) in 10 mM Tris buffer (150 mM NaCl, pH = 7.4).

t ºC	C_L [10^{-3} M]	k_{obs} [10^{-3} s^{-1}]
37.0	5.00	1.50(2)
	4.10	1.30(3)
	3.15	1.10(2)
	2.20	0.93(3)
	1.30	0.77(3)

Table S6. Observed *pseudo*-first order rate constants as a function of complex concentration and temperature for the reaction between complex [Ru(Cl-tpy)Cl_3] (**2**) and L-Met (**L**) in 10 mM Tris buffer (150 mM NaCl, pH = 7.4).

t ºC	C_L [10^{-3} M]	k_{obs} [10^{-3} s^{-1}]
37.0	5.00	0.99(2)
	4.10	0.85(3)
	3.15	0.80(2)
	2.20	0.72(3)
	1.30	0.60(3)

Table S7. Observed *pseudo*-first order rate constants as a function of complex concentration and temperature for the reaction between complex [Ru(Cl-Ph-tpy)Cl_3] (**3**) and 5'-GMP (**L**) in 10 mM Tris buffer (150 mM NaCl, pH = 7.4).

t ºC	C_L [10^{-3} M]	k_{obs} [10^{-3} s^{-1}]
37.0	5.00	12.00(2)
	4.10	9.59(3)
	3.15	8.50(2)
	2.20	6.70(3)
	1.30	5.40(3)

Table S8. Observed *pseudo*-first order rate constants as a function of complex concentration and temperature for the reaction between complex [Ru(Cl-Ph-tpy)Cl_3] (**3**) and L-His (**L**) in 10 mM Tris buffer (150 mM NaCl, pH = 7.4).

t ºC	C_L [10^{-3} M]	k_{obs} [10^{-3} s^{-1}]
37.0	5.00	8.60(2)
	4.10	7.80(3)
	3.15	6.90(2)
	2.20	5.90(3)
	1.30	4.10(3)

Table S9. Observed *pseudo*-first order rate constants as a function of complex concentration and temperature for the reaction between complex [Ru(Cl-Ph-tpy)Cl_3] (**3**) and L-Met (**L**) in 10 mM Tris buffer (150 mM NaCl, pH = 7.4).

t ºC	C_L [10^{-3} M]	k_{obs} [10^{-3} s^{-1}]
37.0	5.00	4.40(2)
	4.10	3.50(3)
	3.15	2.80(2)
	2.20	2.00(3)
	1.30	1.50(3)

Table S10. IC_{50} values (μM) of tested complexes against CT26 cells determined by MTT assay after 24 and 72 hours of exposure presented as mean ±SD.

IC_{50} values (μM)	CT26	
	24 h	72 h
1	50.8 ± 7.2	7.5 ± 2.0
bis-pyrazolylpyridine ligand	146.2 ± 20.9	33.8 ± 7.2
Oxaliplatin	97.1 ± 16.2	3.7 ± 1.0